An Efficient Calibration of MIMO Channel Sounders with Internal Crosstalk

Junseok Kim, *Member, IEEE*, Eun Ae Lee, Chung-Sup Kim, Young-Jun Chong, and Joon Ho Cho, *Member, IEEE*

Abstract—In this paper, a calibration of multiple-input multiple-output (MIMO) channel sounders with internal crosstalk is considered. The objective is to minimize the number of back-to-back (B2B) connections required to estimate the transmitter (Tx) and receiver (Rx) response matrices that convey the information about linear distortion and internal crosstalk. A signal and system model is developed for the B2B measurements, where only some pairs of the Tx and Rx ports of the sounder are utilized among all pairs of the ports. Using the measurement model, a least-square estimation problem is then formulated and converted in the frequency domain to weighted rank-one approximation problems. The notion of system identifiability of a MIMO channel sounder is introduced and some optimal sets of B2B connections are proposed. Given a proposed optimal set of B2B connections, the alternate convex search (ACS) algorithm with a proper initialization is also proposed to solve the weighted rank-one approximation problems. Finally, it is shown how to calibrate field measurement data by using the estimated response matrices. Numerical results show that, only after a couple of iterations, the ACS algorithm with the proposed initialization achieves a comparable identification and calibration performance to the conventional method that requires the B2B connections of all port pairs.

Index Terms—Identifiability, internal crosstalk, MIMO channel sounder calibration, system identification.

I. INTRODUCTION

IN MODERN wireless communications, the use of multiple antennas at the transmitter (Tx) and receiver (Rx) has become a common practice to increase the capacity of a radio link [1], [2]. Standardized channel models that describe such multi-antenna communication links have been thus established [3], [4] to compare different transceiver designs under same conditions. To develop realistic channel models, field measurements are usually conducted in targeted propagation channel environments by using multiple-input multiple-output (MIMO) channel sounders. Then, the channel parameters such as path

J. Kim and E. A. Lee were with the Department of Electrical Engineering (EE), Pohang University of Science and Technology (POSTECH), Pohang, Korea. E. A. Lee is now with Samsung Electronics, Hwaseong, Korea. J. Kim, C.-S. Kim and Y.-J. Chong are with Electronics and Telecommunications Research Institute (ETRI), Daejeon, Korea. J. H. Cho is with the Department of EE, POSTECH (e-mail: jcho@postech.ac.kr).

loss, propagation delay, Doppler frequency shift, the direction of arrival (DOA), and the direction of departure (DOD) are extracted from the measurement data [5], [6].

A fully-parallel MIMO channel sounder is used to sound fast time-varying channels [7], [8]. The Tx has multiple radio-frequency (RF) chains and preceding digital-to-analog converters (DACs) that synchronously perform interpolation of multiple digital baseband, intermediate-frequency (IF), or RF sounding signals. For the multiplexing of the sounding signals, it can employ frequency-division multiplexing (FDM), time-division multiplexing (TDM), or code-division multiplexing (CDM). It is noteworthy that CDM cannot have a less duration for the channel sounding than TDM and FDM at no cost of sounding accuracy [9], [10]. Hence, FDM and TDM are widely adopted due to their simplicity in separating the multiplexed signals. The Rx also has multiple RF chains followed by analog-to-digital converters (ADCs) and makes simultaneous reception of the channel response to the sounding signals. A semi-switched MIMO channel sounder is used to reduce the hardware cost of the Tx by using a single RF chain connected to multiple powered antennas through an RF switch [11], [12]. A fully-switched MIMO channel sounder can further reduce the hardware cost by using a single Rx RF chain but used to sound slowly time-varying channels [13]–[17].

All these MIMO channel sounders have multiple antennas and RF paths, which may cause impairments to be compensated for. To compensate for antenna coupling, the coupling scattering coefficients of the antenna arrays are typically measured in an anechoic chamber [18]. To compensate for internal impairments such as the frequency-selectivity of the RF paths, the Tx and Rx are typically back-to-back (B2B) connected after removing the antennas, and then the response of the B2B-connected sounder is measured to perform system identification [9], [10], [19]–[22]. Using the system responses and coupling coefficients, the data obtained from the field measurement campaigns are adjusted and the channel parameters are estimated. Internal crosstalk is an impairment that is caused by the leakage of the signals that pass through different RF paths [23], [24]. It becomes severer, e.g., in a milimeter-wave massive MIMO system, as the operating frequency increases and the paths are packed more densely.

The compensation of such impairments is also needed for MIMO *communication systems*. Especially in time-division duplexing, it is crucial to restore channel reciprocity [25]. Hence, much research has been conducted. However, either the internal crosstalk is not taken into account [26]–[29] or Tx calibration is mainly considered because the system response of the Rx can be absorbed in the overall channel response

during the demodulation [24], [30]–[37].

For MIMO *channel sounders*, on the contrary, Rx calibration is also important to extract the channel parameters accurately. This is because the propagation channel response goes between the Tx and Rx responses with the internal crosstalk, and commutativity does not hold in this cascade of the responses as it does not hold in general for the multiplication of three matrices. Unlike most of the papers about the calibration of channel sounders without internal crosstalk [9], [10], [19], our recent work has proposed a joint Tx and Rx calibration method for a MIMO channel sounder with internal crosstalk [17]. However, the method requires B2B connections for all $N_T N_R$ pairs of the Tx and Rx ports, where N_T and N_R are the number of Tx and Rx ports, respectively. Hence, it has the number of B2B connections growing very fast as N_T and N_R increase. Moreover, it leaves the problems unanswered on what is the minimum number of B2B connections that is necessary for the separate system identification of the Tx and Rx, and on what is an optimal set of test channels associated with the minimum number.

Over-the-air (OTA) measurements are not considered in [17]. Unlike B2B measurements, OTA measurements require no extra hardware or labor. Moreover, OTA measurements may be the only way for some MIMO *communication systems*, where it is difficult to remove antennas from the transceivers [26]–[29]. However, no method with OTA measurements is proposed yet for the compensation of the internal crosstalk at both the Tx and Rx, because identifying the OTA test channel becomes a problem as hard as the original problem of identifying the MIMO channel sounder. Fortunately, channel sounders are usually designed to allow the separation of the antennas from the RF chains for the test of various antennas, which is also assumed in this paper.

In this paper, we investigate the problem on the minimum number of B2B connections, which may provide a great benefit to the calibration of massive MIMO channel sounders. The Tx and Rx of the channel sounder are modeled by MIMO linear time-invariant systems with *non-diagonal* impulse response matrices. Nonlinear crosstalk [34] and distortion are not considered because the signals fed to the power amplifiers (PAs) and low-noise amplifiers (LNAs) of a channel sounder are usually of low peak-to-average power ratio (PAPR) and carefully conditioned in order to make the amplifiers operate in the linear region.

Specifically when TDM is employed for the multiplexing of the sounding signals during the B2B measurements, we formulate a least-square (LS) system identification problem to find the estimates of the Tx and Rx response matrices. It is shown that the problem can be converted to weighted rank-one approximation problems to be solved in each frequency bin of interest. We introduce the notion of identifiability of the channel sounder, derive certain conditions on a set of B2B connections to make the sounder identifiable, and provide some optimal sets. It turns out that the minimum number of connections is $N_T + N_R - 1$, which is the same number of connections required by the method in [19] that can calibrate only a MIMO channel sounder *without* internal crosstalk. We propose to solve the formulated LS problem

by using the alternate convex search (ACS) algorithm, as ordinary weighted rank-one approximation problems are often solved by ACS algorithms. However, the rate of convergence to reliable estimates of the response matrices strongly depend on initial estimates. Hence, we also propose an accompanying initialization scheme that leads to a fast convergence of the ACS algorithm for the optimal sets. Finally, it is shown how to calibrate field measurement data by using the estimated response matrices. Numerical results show that only a couple of iterations are enough to obtain the estimates as reliable as those in [17], where $N_T N_R$ B2B connections are required to compensate for the internal crosstalk.

The rest of this paper is organized as follows. In Section II, signal and system model that incorporates the effect of the internal crosstalk is described for the fully-parallel MIMO channel sounder. In Section III, a B2B connection to obtain measurement data is introduced and an LS system identification problem is formulated. In Section IV, the identifiability of the MIMO channel sounder is investigated, the minimum number of B2B connections is derived, and the formulated LS system identification problem is solved. In Section V, it is discussed how to calibrate the field measurement data to estimate the channel. Complexity issues are also discussed. Then, simulation results are provided. Finally, concluding remarks are offered in Section VI.

Throughout this paper, $*$ denotes the convolution, $\mathrm{mod}(\cdot, n)$ denotes the modulo-n operation, and $|\cdot|$ denotes the cardinality of a set. The matrices $\boldsymbol{O}_{N_R \times N_T}$ and $\boldsymbol{1}_{N_R \times N_T}$ denote the N_R-by-N_T all-zero matrix and the N_R-by-N_T all-one matrix, respectively, and $\mathcal{V}(\cdot)$ denotes the vectorization operation that stacks the columns of the argument matrix to generate a vector. The superscripts $(\cdot)^*$, $(\cdot)^{\mathcal{T}}$, and $(\cdot)^{\mathcal{H}}$ denote the conjugate, the transpose, and the conjugate transpose, respectively, and $[\cdot]_{i,j}$, $\mathrm{tr}(\cdot)$, and $\|\cdot\|_F$ denote the (i,j)th entry, the trace, and the Frobenius norm of a matrix, respectively. The operators $\odot$ and $\otimes$ denote the Hadamard product and the Kronecker product, respectively. To describe the computational complexity, we will use the big-$\mathcal{O}$ notation $\mathcal{O}(g(N))$ defined as $f(N) = \mathcal{O}(g(N))$ if and only if there exist a positive constant M and a real number N_0 such that $|f(N)| \leq M|g(N)|, \forall N > N_0$.

II. SIGNAL AND SYSTEM MODEL

In this section, we describe signal and system model. The model well takes into account not only the linear time-invariant distortion within an RF path but also the internal crosstalk between RF paths in the Tx and Rx.

Fig. 1-(a) shows the block diagram of the parallel channel sounder in complex baseband. The sounder is composed of N_T RF chains and N_T antennas in the Tx, and N_R antennas and N_R RF chains in the Rx, which enables simultaneous transmission and reception of sounding signals through multiple RF ports.

The vector-valued sounding signal $\boldsymbol{s}(t)$ given by

$$\boldsymbol{s}(t) \triangleq \begin{bmatrix} s_1(t), s_2(t), \cdots, s_{N_T}(t) \end{bmatrix}^{\mathcal{T}} \tag{1}$$

consists of N_T scalar-valued sounding signals, each of which is applied to each Tx RF port. The ith sounding signal $s_i(t)$,
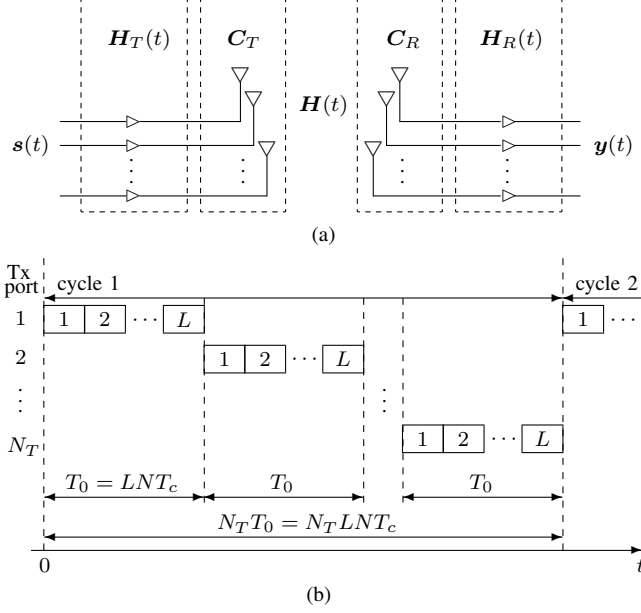
Fig. 1. (a) Signal and system model of a fully-parallel MIMO channel sounder, and (b) typical timing structure of TDM-based transmission at Tx.

for $i = 1, 2, \cdots, N_T$, mainly passes through the ith Tx RF chain and the ith powered Tx antenna, but there is some linear time-invariant distortion and leakage to other RF paths. The N_T-by-N_T matrix-valued function $\boldsymbol{H}_T(t)$ called the Tx response matrix models the above impairments, where the (j, l)th entry is the impulse response from the input of the lth RF chain to the output of the jth PA at the Tx, for $j, l = 1, 2, \cdots, N_T$. To separately handle the coupling due to the imperfect Tx antennas, the N_T-by-N_T antenna coupling matrix $\boldsymbol{C}_T$ is introduced.

The transmitted signal passes through the MIMO channel with an N_R-by-N_T impulse response $\boldsymbol{H}(t)$. Similar to $\boldsymbol{C}_T$ and $\boldsymbol{H}_T(t)$, the N_R-by-N_R matrices $\boldsymbol{C}_R$ and $\boldsymbol{H}_R(t)$ are defined as the Rx antenna coupling matrix and the Rx response matrix, respectively. Specifically, the (i, k)th entry of $\boldsymbol{H}_R(t)$ is the impulse response from the input of the kth LNA at the Rx to the output of the ith Rx chain, for $i, k = 1, 2, \cdots, N_R$.

Thus, the vector-valued received signal denoted by

$$\boldsymbol{y}(t) \triangleq \begin{bmatrix} y_1(t), y_2(t), \cdots, y_{N_R}(t) \end{bmatrix}^{\mathcal{T}} \qquad (2a)$$

can be written as

$$\boldsymbol{y}(t) = \boldsymbol{H}_R(t) * \{\boldsymbol{C}_R \boldsymbol{H}(t) \boldsymbol{C}_T\} * \boldsymbol{H}_T(t) * \boldsymbol{s}(t) + \boldsymbol{n}(t), \quad (2b)$$

where $\boldsymbol{n}(t)$ is an N_R-by-1 additive Gaussian noise.

The objective of the channel sounding is to extract the parameters of a propagation channel from $\boldsymbol{y}(t)$ by estimating $\boldsymbol{H}(t)$. However, as (2b) clearly shows, this cannot be done without the information on the Tx and Rx response matrices $\boldsymbol{H}_T(t)$ and $\boldsymbol{H}_R(t)$, and the antenna coupling matrices $\boldsymbol{C}_T$ and $\boldsymbol{C}_R$. The antenna coupling matrices are assumed to be estimated through a separate measurement performed in an anechoic chamber. Thus, $\boldsymbol{H}_T(t)$ and $\boldsymbol{H}_R(t)$ are estimated

based on the B2B measurements, and $\boldsymbol{H}(t)$ is estimated based on the field measurements. In the rest of this section, we describe the TDM-based sounding signal in detail, which can be used both in the B2B and field measurements without compromising the sounding duration [9], [10].

Suppose that a scalar-valued discrete-time (DT) periodic signal $b[n] = b[n+N], \forall n$, such as an m-sequence with period N is time-division multiplexed to construct the vector-valued sounding signal

$$\boldsymbol{s}(t) = \sum_{n=-\infty}^{\infty} b[n] \boldsymbol{w}_T[n] p(t - nT_c), \qquad (3a)$$

where $\boldsymbol{w}_T[n]$ is an N_T-by-1 vector-valued windowing function that effectively switches the transmitting port at every Lth period of $b[n]$, $p(t)$ is a transmit pulse, and $1/T_c$ is the chip rate. Usually, a square-root Nyquist pulse with excess bandwidth $0 < \alpha < 1$ is employed as $p(t)$ such that

$$B < \frac{1 + \alpha}{2T_c}, \qquad (3b)$$

where B is the bandwidth in complex baseband of the channel to be sounded. This choice is to ensure that every frequency of the channel of interest is probed at sufficiently large signal power.

Let

$$T_0 \triangleq LNT_c \qquad (3c)$$

be the period of the switching performed by the windowing function. Then, $\boldsymbol{w}_T[n]$ is given by

$$\boldsymbol{w}_T[n] \triangleq \sum_{m=-\infty}^{\infty} \boldsymbol{e}_{\text{mod}(m, N_T)+1}^{(N_T)} \Pi_{LN}[n - mLN], \quad (3d)$$

where $\boldsymbol{e}_m^{(n)}$ is the mth standard basis vector of $\mathbb{R}^n$ and $\Pi_{LN}[n]$ is the DT rectangular pulse with non-zero support $n \in \{0, 1, \cdots, LN - 1\}$. Whenever there is no confusion, the superscript of $\boldsymbol{e}_m^{(n)}$ will be dropped for notational convenience. As seen in Fig. 1-(b), an equal-length time slot of duration T_0 seconds is provided to each transmit port under round-robin scheduling during one sounding cycle of $N_T T_0$ seconds. Each slot consists of L periods of the signal but, usually, the first and last periods among the L periods are not used in the estimation to remove the effects of the discontinuities of the windowing function at the edges of the slot.

In the next section, we propose how to identify $\boldsymbol{H}_T(t)$ and $\boldsymbol{H}_R(t)$ from the measurement data obtained via B2B connections between the Tx and Rx.

III. B2B MEASUREMENTS AND SYSTEM IDENTIFICATION

In this section, under the assumption that the sounding signal is TDM-based, we describe how to make B2B connections to obtain measurement data and how to formulate an LS system identification problem to estimate the Tx and Rx response matrices.
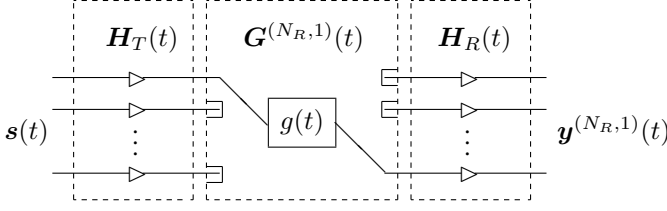
Fig. 2. Signal and system model when the 1st PA output and the N_Rth LNA input are connected via a delay line.

A. B2B Measurements

A typical system identification problem involves designing a system input called a test signal, applying the test signal as the input to the system, and making a measurement at the system output. Then, an estimation problem, which is basically an optimization problem, is formulated and solved [38]. Unlike the typical system identification problems, our identification problem has *two* systems to be identified that reflect the internal responses in the Tx and Rx of the MIMO channel sounder. Moreover, the two systems are not directly connected but indirectly connected through a channel. Of course, the Tx and Rx response matrices can be separately identified by performing two separate ordinary system identification procedures. For example, the response between an input RF port and an output RF port can be measured by using a vector network analyzer (VNA). However, such a procedure requires to perform $N_T^2 + N_R^2$ measurements to identify the response matrices for the MIMO channel sounder. Moreover, such a procedure requires to disassemble many parts of the sounder.

To perform the system identification for a MIMO channel sounder, B2B measurements are often performed that require only to remove the Tx and Rx antenna elements and to connect an output RF port of the Tx with an input RF port of the Rx using a channel having a known response [19], [20]. We do not consider using a calibration kit such as that employed in [10] to facilitate the B2B measurements, because crosstalk may occur inside the calibration kit consisting of densely-packed RF paths and switches. Usually, a single-input single-output delay line consisting of a cable, an attenuator, and a cable with very high RF shielding is used for a B2B connection as a known channel, where all other input and output ports are properly terminated. Such a channel is called a *test channel* and it is obvious that more than one B2B connections should be made to identify the Tx and Rx response matrices of a MIMO channel sounder. Thus, to identify the response matrices, a set of *test channels* should be designed as well as the test signal.

In this paper, we consider using the same test signal for all B2B measurements. In particular, the TDM-based sounding signal defined in (3) is used. This test signal may have a much shorter period than the sounding signal used for the field measurements because the delay spread of the delay line is much smaller than that of a wireless channel in general.

Fig. 2 illustrates an exemplary test channel where the N_Rth LNA input and the 1st PA output are connected via a delay line. If the ith LNA input and the jth PA output are connected,

then $\boldsymbol{C}_R \boldsymbol{H}(t) \boldsymbol{C}_T$ in (2b) can be replaced by

$$\boldsymbol{G}^{(i,j)}(t) \triangleq g(t) \boldsymbol{e}_i^{(N_R)} (\boldsymbol{e}_j^{(N_T)})^{\mathcal{T}}, \tag{4}$$

where $g(t)$ is the known impulse response of the delay line. Accordingly, the complex envelope of the output of the Rx ports during this (i,j)th B2B measurement is denoted by $\boldsymbol{y}^{(i,j)}(t)$.

The complex envelope $\boldsymbol{y}^{(i,j)}(t)$ of the output of the Rx RF port passes through the chip-matched filter with impulse response $p(-t)^*$ and the filter output $\boldsymbol{z}^{(i,j)}(t) \triangleq p(-t)^* * \boldsymbol{y}^{(i,j)}(t)$ is oversampled at every $T_s \triangleq T_c/M$ second to generate $(\boldsymbol{z}^{(i,j)}[m])_m$, i.e.,

$$\boldsymbol{z}^{(i,j)}[m] \triangleq \boldsymbol{z}^{(i,j)}(mT_s) = p(-t)^* * \boldsymbol{y}^{(i,j)}(t)\big|_{t=m\frac{T_c}{M}} \tag{5}$$

for $m = 0, 1, \cdots, LMNN_T - 1$, where $M \in \mathbb{N}$ is chosen to make the sampling rate $1/T_s \triangleq M/T_c$ high enough to cause no aliasing within the channel frequency band of interest.

Unlike [17], we do not necessarily consider making all $N_T N_R$ B2B measurements, i.e., we do not use the test channel for all pairs of i and j. Thus, we formulate a new LS system identification problem now with a general set of test channels in the next subsection.

B. System Identification Problem Formulation

Let $\mathbb{S}$ be the subset of (i,j) pairs with which the B2B measurement $\boldsymbol{z}^{(i,j)}[m]$ is available. Since all $N_T N_R$ (i,j) pairs may not be included in $\mathbb{S}$, the cardinality $|\mathbb{S}|$ satisfies $|\mathbb{S}| \leq N_T N_R$ in general. Given $\mathbb{S}$, called the set of test channels or the set of B2B connections, an LS problem to find the best estimates of the response matrices is formulated as follows.

As already seen in Fig. 1-(b), there are N_T slots in a cycle. Now, each slot has the LMN samples of the chip-matched filter output vectors $\boldsymbol{z}^{(i,j)}[m]$ of length-N_R. By removing the first and last periods and averaging the chip-matched filter outputs for the rest $L-2$ periods to enhance the signal-to-noise ratio (SNR), we can rearrange $\boldsymbol{z}^{(i,j)}[m]$ for $m = 0, 1, \cdots, LMNN_T - 1$ slot-by-slot as an $N_R \times N_T \times MN$ tensor $\boldsymbol{Z}^{(i,j)}$ or, equivalently, N_R-by-N_T matrices $\boldsymbol{Z}^{(i,j)}[m]$ for $m = 0, 1, \cdots, MN - 1$, whose (k,l)th element is given by

$$(\boldsymbol{e}_k^{(N_R)})^{\mathcal{T}} \boldsymbol{Z}^{(i,j)}[m] \boldsymbol{e}_l^{(N_T)} \triangleq \frac{1}{L-2} \sum_{n=1}^{L-2} (\boldsymbol{e}_k^{(N_R)})^{\mathcal{T}} \boldsymbol{z}^{(i,j)}[m$$
$$+ nMN + (l-1)LMN]. \tag{6a}$$

If more than a single cycle is observed, $\boldsymbol{Z}^{(i,j)}[m]$ can be obtained by averaging the samples over the cycles in order to further enhance the SNR.

To represent $\boldsymbol{Z}^{(i,j)}[m]$ with the Tx and Rx response matrices, the sampled versions of the signal and system responses are defined as $x[m] \triangleq p(-t)^* * s(t)|_{t=mT_s}$, $\boldsymbol{H}_T[m] \triangleq \boldsymbol{H}_T(mT_s)$, $\boldsymbol{G}^{(i,j)}[m] \triangleq \boldsymbol{G}^{(i,j)}(mT_s)$, and $\boldsymbol{H}_R[m] \triangleq \boldsymbol{H}_R(mT_s)$. If N is large enough that N is greater than or equal to the largest delay of the components in $\boldsymbol{z}^{(i,j)}[m]$, then $\boldsymbol{Z}^{(i,j)}[m]$ can be approximately written by

$$\boldsymbol{Z}^{(i,j)}[m] = T_s^3 \big(\boldsymbol{H}_R[m] * \boldsymbol{G}^{(i,j)}[m] * \boldsymbol{H}_T[m] \big) * x[m]$$
$$+ \boldsymbol{N}^{(i,j)}[m], \tag{6b}$$

for $m = 0, 1, \cdots, MN - 1$, where $*$ denotes the convolution sum and $\boldsymbol{N}^{(i,j)}[m]$ is an N_R-by-N_T matrix-valued noise component in $\boldsymbol{Z}^{(i,j)}[m]$.

A rearrangement of the received signal similar to (6b) can be applied to a semi-switched sounder and a fully-switched sounder with a periodic test signal. For example, it is shown in [17] that, although the timing structure of a test signal is different from that in Fig. 1-(b), a fully-switched sounder has almost the same relation as (6b) among the sampled versions of the signals and system responses. Thus, the following LS system identification problem that utilizes $\boldsymbol{Z}^{(i,j)}[m]$ only for some (i,j) pairs among $N_T N_R$ pairs can also be formulated for semi-switched and fully-switched sounders.

As a typical LS system identification problem employs a model error function whose power is to be minimized, we employ model error functions

$$
\begin{aligned}
\boldsymbol{E}^{(i,j)}[m] &\triangleq \boldsymbol{Z}^{(i,j)}[m] \\
&- T_s^3 \left(\boldsymbol{U}[m] * \boldsymbol{G}^{(i,j)}[m] * \boldsymbol{V}[m] \right) * x[m], \quad (7a)
\end{aligned}
$$

for $m = 0, 1, \cdots, MN - 1$ and $(i,j) \in \mathbb{S}$, and formulate the LS system identification problem in the time domain (TD) as

$$
(\hat{\boldsymbol{H}}_R[m], \hat{\boldsymbol{H}}_T[m])_m \triangleq
$$
$$
\underset{(\boldsymbol{U}[m], \boldsymbol{V}[m])_m}{\operatorname{argmin}} \sum_{(i,j) \in \mathbb{S}} \sum_{m=0}^{MN-1} \left\| \boldsymbol{E}^{(i,j)}[m] \right\|_F^2, \quad (7b)
$$

where the sequence $(\hat{\boldsymbol{H}}_R[m], \hat{\boldsymbol{H}}_T[m])_m$ is the estimate of $(\boldsymbol{H}_R[m], \boldsymbol{H}_T[m])_m$.

Now, the error functions and the objective function in (7) are rewritten in the frequency domain (FD).

Lemma 1: Let $\tilde{\boldsymbol{E}}^{(i,j)}[k]$, $\tilde{\boldsymbol{Z}}^{(i,j)}[k]$, and $\tilde{x}[k]$ be the unitary discrete Fourier transforms (DFTs) of $\boldsymbol{E}^{(i,j)}[m]$, $\boldsymbol{Z}^{(i,j)}[m]$, and $x[m]$ respectively. Also, let $\tilde{\boldsymbol{U}}[k]$, $\tilde{g}[k]$, and $\tilde{\boldsymbol{V}}[k]$ be the discrete-time Fourier transforms (DTFTs) of $\boldsymbol{U}[m]$, $g(mT_s)$, and $\boldsymbol{V}[m]$ evaluated at $f = k/(MN)$, respectively. Then, we have

$$
\begin{aligned}
\tilde{\boldsymbol{E}}^{(i,j)}[k] &= \tilde{\boldsymbol{Z}}^{(i,j)}[k] \\
&- T_s^3 \tilde{g}[k] \tilde{x}[k] \tilde{\boldsymbol{U}}[k] \boldsymbol{e}_i^{(N_R)} (\boldsymbol{e}_j^{(N_T)})^{\mathcal{T}} \tilde{\boldsymbol{V}}[k] \quad (8a)
\end{aligned}
$$

and

$$
\sum_{(i,j) \in \mathbb{S}} \sum_{m=0}^{MN-1} \left\| \boldsymbol{E}^{(i,j)}[m] \right\|_F^2 = \sum_{(i,j) \in \mathbb{S}} \sum_{k=0}^{MN-1} \left\| \tilde{\boldsymbol{E}}^{(i,j)}[k] \right\|_F^2. \quad (8b)
$$

Proof: Omitted. See a similar proof in [17, *Lemma 1*]. $\square$

This lemma enables a reformulation in the FD of the LS problem as

$$
(\check{\boldsymbol{H}}_R[k], \check{\boldsymbol{H}}_T[k])_k \triangleq \underset{(\tilde{\boldsymbol{U}}[k], \tilde{\boldsymbol{V}}[k])_k}{\operatorname{argmin}} \sum_{(i,j) \in \mathbb{S}} \sum_{k=0}^{MN-1} \left\| \tilde{\boldsymbol{E}}^{(i,j)}[k] \right\|_F^2, \quad (9)
$$

where $\check{\boldsymbol{H}}_R[k]$ and $\check{\boldsymbol{H}}_T[k]$ are the estimates of $\tilde{\boldsymbol{H}}_R[k]$ and $\tilde{\boldsymbol{H}}_T[k]$, respectively, which are the DTFTs of $\boldsymbol{H}_R[m]$ and $\boldsymbol{H}_T[m]$ evaluated at $f = k/(MN)$. As shown in [17], if $\mathbb{S}$ includes all $N_T N_R$ (i,j) pairs, the above FD problem can be converted to rank-one approximation problems to be solved at each frequency bin k. However, it is not the case in our

problem. Thus, in the following proposition, we introduce the notions of weight matrix and blockwise weight matrix and convert (9) into weighted rank-one approximation problems [39].

Proposition 1: Let $\tilde{\boldsymbol{Z}}[k]$ be the N_R^2-by-N_T^2 matrix obtained by putting together the N_R-by-N_T matrices $\tilde{\boldsymbol{Z}}^{(i,j)}[k]$ for $i = 1, 2, \cdots, N_R$ and $j = 1, 2, \cdots, N_T$ as

$$
\tilde{\boldsymbol{Z}}[k] \triangleq \begin{bmatrix}
\tilde{\boldsymbol{Z}}^{(1,1)}[k] & \tilde{\boldsymbol{Z}}^{(1,2)}[k] & \cdots & \tilde{\boldsymbol{Z}}^{(1,N_T)}[k] \\
\tilde{\boldsymbol{Z}}^{(2,1)}[k] & \tilde{\boldsymbol{Z}}^{(2,2)}[k] & \cdots & \tilde{\boldsymbol{Z}}^{(2,N_T)}[k] \\
\vdots & \vdots & \ddots & \vdots \\
\tilde{\boldsymbol{Z}}^{(N_R,1)}[k] & \tilde{\boldsymbol{Z}}^{(N_R,2)}[k] & \cdots & \tilde{\boldsymbol{Z}}^{(N_R,N_T)}[k]
\end{bmatrix},
$$
$$
\quad (10)
$$

for $k = 0, 1, \cdots, MN - 1$. Here,

$$
\tilde{\boldsymbol{Z}}^{(i,j)}[k] \triangleq \boldsymbol{O}_{N_R \times N_T} \quad (11)
$$

for $(i,j) \notin \mathbb{S}$ and $k = 0, 1, \cdots, MN - 1$.

Then, the joint optimization problem in (9) can be rewritten as

$$
\begin{aligned}
(\check{\boldsymbol{h}}_R[k], \check{\boldsymbol{h}}_T[k])_k &\triangleq \underset{(\tilde{\boldsymbol{u}}[k], \tilde{\boldsymbol{v}}[k])_k}{\operatorname{argmin}} \sum_{k=0}^{MN-1} \left\| \boldsymbol{W} \odot \left\{ \tilde{\boldsymbol{Z}}[k] \right. \right. \\
&\left. \left. - T_s^3 \tilde{x}[k] \tilde{g}[k] \tilde{\boldsymbol{u}}[k] \tilde{\boldsymbol{v}}[k]^{\mathcal{T}} \right\} \right\|_F^2, \quad (12a)
\end{aligned}
$$

where the length-N_R^2 column vectors $\check{\boldsymbol{h}}_R[k]$ and $\tilde{\boldsymbol{u}}[k]$, and the length-$N_T^2$ column vectors $\check{\boldsymbol{h}}_T[k]$ and $\tilde{\boldsymbol{v}}[k]$ are defined by

$$
\check{\boldsymbol{h}}_R[k] \triangleq \mathcal{V}(\check{\boldsymbol{H}}_R[k]), \quad \tilde{\boldsymbol{u}}[k] \triangleq \mathcal{V}(\tilde{\boldsymbol{U}}[k]) \quad (12b)
$$

and

$$
\check{\boldsymbol{h}}_T[k] \triangleq \mathcal{V}(\check{\boldsymbol{H}}_T[k]^{\mathcal{T}}), \quad \tilde{\boldsymbol{v}}[k] \triangleq \mathcal{V}(\tilde{\boldsymbol{V}}[k]^{\mathcal{T}}), \quad (12c)
$$

for $k = 0, 1, \cdots, MN - 1$. Here, $\check{\boldsymbol{h}}_R[k]$ and $\check{\boldsymbol{h}}_T[k]$ are the estimates of $\tilde{\boldsymbol{h}}_R[k] \triangleq \mathcal{V}(\tilde{\boldsymbol{H}}_R[k])$ and $\tilde{\boldsymbol{h}}_T[k] \triangleq \mathcal{V}(\tilde{\boldsymbol{H}}_T[k])$, respectively. The N_R^2-by-N_T^2 matrix $\boldsymbol{W}$ called a weight matrix has entries in $\{0, 1\}$ such that

$$
\boldsymbol{W} \triangleq \boldsymbol{B} \otimes \boldsymbol{1}_{N_R \times N_T}, \quad (13a)
$$

where $\boldsymbol{B}$ is an N_R-by-N_T matrix called a blockwise weight matrix defined as

$$
[\boldsymbol{B}]_{i,j} \triangleq \begin{cases} 1 & \text{if } (i,j) \in \mathbb{S} \\ 0 & \text{if } (i,j) \notin \mathbb{S} \end{cases} \quad (13b)
$$

for $i = 1, 2, \cdots, N_R$ and $j = 1, 2, \cdots, N_T$.

Proof: If every pair (i,j) of the B2B measurement $\boldsymbol{Z}^{(i,j)}[m]$ is available for $i = 1, 2, \cdots, N_R$ and $j = 1, 2, \cdots, N_T$, we can show by using [17, *Proposition 1*] that the joint optimization problem can be rewritten as

$$
\begin{aligned}
(\check{\boldsymbol{h}}_R[k], \check{\boldsymbol{h}}_T[k])_k &\triangleq \underset{(\tilde{\boldsymbol{u}}[k], \tilde{\boldsymbol{v}}[k])_k}{\operatorname{argmin}} \sum_{k=0}^{MN-1} \left\| \tilde{\boldsymbol{Z}}[k] \right. \\
&\left. - T_s^3 \tilde{x}[k] \tilde{g}[k] \tilde{\boldsymbol{u}}[k] \tilde{\boldsymbol{v}}[k]^{\mathcal{T}} \right\|_F^2. \quad (14)
\end{aligned}
$$

If not, then we can straightforwardly modify (14) as (12a) by adopting the weight matrix $\boldsymbol{W}$ defined by (13). Therefore, the conclusion follows. $\square$

The objective function in (12a) can be minimized by minimizing each frequency term. Hence, the problem (12a)

becomes MN separate minimization problems. However, we just need to solve

$$(\check{\boldsymbol{h}}_R[k], \check{\boldsymbol{h}}_T[k]) \triangleq \underset{(\tilde{\boldsymbol{u}}[k], \tilde{\boldsymbol{v}}[k])}{\operatorname{argmin}} \left\| \boldsymbol{W} \odot \big\{ \tilde{\boldsymbol{Z}}[k] \right.$$
$$\left. - T_s^3 \tilde{x}[k] \tilde{g}[k] \tilde{\boldsymbol{u}}[k] \tilde{\boldsymbol{v}}[k]^{\mathcal{T}} \big\} \right\|_F^2 \quad (15)$$

only for some k. This is because there are k's that correspond to the frequencies outside the frequency band of the channel to be sounded. It is assumed that $T_s^3 \tilde{x}[k] \tilde{g}[k] \neq 0$ for all k's corresponding to the frequencies inside the band of interest.

Note that the LS system identification problem in (15), after its objective function being scaled by $|T_s^3 \tilde{x}[k] \tilde{g}[k]|^2$, becomes nothing but a weighted rank-one approximation problem [39], where the weight 0 is used to take missing data into account.

In the next section, we find the necessary and sufficient condition for $\mathbb{S}$ to make the system identifiable and derive the minimum number of test channels required for the system identifiability. Then, we solve the weighted rank-one approximation problems in (15).

IV. IDENTIFIABILITY, MINIMUM NUMBER OF B2B CONNECTIONS, AND SOLUTION TO IDENTIFICATION PROBLEM

In this section, we investigate the identifiability of the channel sounder and derive the minimum number of B2B connections to satisfy the identifiability. Then, we provide a numerical solution along with an initialization scheme to the system identification problem (15).

A. Identifiability of MIMO Channel Sounder

The choice of $\boldsymbol{W} = \boldsymbol{B} \otimes \mathbf{1}_{N_R \times N_T}$, equivalently, the choice of $\mathbb{S}$ is very important for the identification of the MIMO channel sounder. This is because for some choices of $\mathbb{S}$ the estimates of $(\tilde{\boldsymbol{h}}_R[k], \tilde{\boldsymbol{h}}_T[k])_k$ as the solutions to the separate LS problems in (15) become meaningless. For example, if $[\boldsymbol{B}]_{i,j} = 0$ for all (i, j) except $[\boldsymbol{B}]_{1,1} = 1$, all the columns of $\check{\boldsymbol{H}}_R[k]$ except the first column and all the rows of $\check{\boldsymbol{H}}_T[k]$ except the first row can be arbitrarily chosen without changing the objective function value of (15). In this case, an LS estimate is meaningless even if the squared error is minimized by the estimate.

To avoid such a meaningless estimate, the notion of system identifiability has already been developed in the ordinary system identification [38, Sec. 2.1]. This notion is motivated by the model identifiability in statistics [40, Def. 1.5.2], and can be modified as follows specifically for our MIMO channel sounder with the test signal model, the test channels, and the LS criterion described in the previous section.

Definition 1: Given the input-parameter-output relation in (6b), a set $\mathbb{S}$ of test channels, the test signal $\boldsymbol{s}(t)$ in (3), and the LS estimator that solves (15), the MIMO channel sounder is called *identifiable* if

D1) the mapping between the parameters and the probability distribution of the outputs is one-to-one, and

D2) the estimator is consistent in the sense that the estimate converges to the true value of the parameters as the number of observations tends to infinity,

where Conditions D1) and D2) are satisfied under scalar ambiguity.

A major difference from the ordinary system identifiability is that the identifiability of the MIMO channel sounder is an ability not only of the input-parameter-output relation, the test signal, and the optimality criterion, but also of the *test channels*. Another major difference is that Conditions D1) and D2) are relaxed to allow a scalar ambiguity. For Condition D1), this means that two parameter pairs $(\tilde{\boldsymbol{H}}_R[k], \tilde{\boldsymbol{H}}_T[k])$ and $(\beta[k] \tilde{\boldsymbol{H}}_R[k], (1/\beta[k]) \tilde{\boldsymbol{H}}_T[k])$ are regarded equivalent for any non-zero scalar $\beta[k]$. This relaxation is justified because $(\beta[k] \tilde{\boldsymbol{H}}_R[k], (1/\beta[k]) \tilde{\boldsymbol{H}}_T[k])$ generates the same probability distribution of the system output for all $\beta[k] \neq 0$ during the B2B measurements. For Condition D2), this means that the estimate pair $(\check{\boldsymbol{H}}_R[k], \check{\boldsymbol{H}}_T[k])$ converges to $(\beta[k] \tilde{\boldsymbol{H}}_R[k], (1/\beta[k]) \tilde{\boldsymbol{H}}_T[k])$ for some non-zero scalar $\beta[k]$.

Lemma 2: Condition D1) is satisfied if and only if, for each k, there is a one-to-one correspondence between $(\tilde{\boldsymbol{H}}_R[k], \tilde{\boldsymbol{H}}_T[k])$ and

$$\boldsymbol{M}[k] \triangleq \boldsymbol{W} \odot \tilde{\boldsymbol{h}}_R[k] \tilde{\boldsymbol{h}}_T[k]^{\mathcal{T}}, \quad (16)$$

under scalar ambiguity.

Proof: Given a weight matrix $\boldsymbol{W}$, the observation $\tilde{\boldsymbol{Z}}[k]$ becomes a Gaussian random matrix with mean matrix $\boldsymbol{W} \odot T_s^3 \tilde{x}[k] \tilde{g}[k] \tilde{\boldsymbol{h}}_R[k] \tilde{\boldsymbol{h}}_T[k]^{\mathcal{T}}$. Since the correlation among the noise components of $\tilde{\boldsymbol{Z}}[k]$ are not affected by $(\tilde{\boldsymbol{H}}_R[k], \tilde{\boldsymbol{H}}_T[k])$, a one-to-one correspondence between $(\tilde{\boldsymbol{H}}_R[k], \tilde{\boldsymbol{H}}_T[k])$ and the distribution of $\tilde{\boldsymbol{Z}}[k]$ is equivalent to a one-to-one correspondence between $(\tilde{\boldsymbol{H}}_R[k], \tilde{\boldsymbol{H}}_T[k])$ and the mean matrix under scalar ambiguity. Therefore, the conclusion follows because it is assumed that $T_s^3 \tilde{x}[k] \tilde{g}[k] \neq 0$ for all k's inside the frequency band of interest. $\square$

In the rest of this subsection, we first investigate Condition D1), i.e., we find a necessary and sufficient condition for $\mathbb{S}$, equivalently, for $\boldsymbol{W}$ to satisfy Condition D1). Then, we show that the LS estimates satisfy Condition D2), when $\mathbb{S}$ satisfies Condition D1). Thus, the necessary and sufficient condition for $\mathbb{S}$ to satisfy Condition D1) is actually the necessary and sufficient condition for $\mathbb{S}$ to make the system identifiable.

Definition 2: A pair $(i, j) \in \mathbb{S}$ of the Rx and Tx RF ports is called *connected* to $(i', j') \in \mathbb{S}$ if there exists a length-P sequence $(a_p, b_p)_p$ for $p = 1, 2, \cdots, P < \infty$ such that $a_{p+1} = a_p$ or $b_{p+1} = b_p$ for all $p = 1, 2, \cdots, P-1$, where all the sequence elements are from $\mathbb{S}$, $(a_1, b_1) = (i, j)$ and $(a_P, b_P) = (i', j')$.

In what follows, $(i, j) \sim (i', j')$ and $(i, j) \nsim (i', j')$ will denote, respectively, that the pairs are connected and not connected. From the definition, it can be easily seen that $(i, j) \sim (i, j)$, and that $(i, j) \sim (i', j') \iff (i', j') \sim (i, j)$.

Some consequences of the above definitions are as follows. To proceed, define additionally $\mathbb{S}^{(i,j)}$ and $\overline{\mathbb{S}}^{(i,j)}$ as the sets of every $(i', j') \in \mathbb{S}$ connected to (i, j) and not connected to (i, j), respectively. Also, define $\mathbb{S}_x$ and $\mathbb{S}_y$ as $\mathbb{S}_x \triangleq \{x : (x, y) \in \mathbb{S}, \exists y\}$ and $\mathbb{S}_y \triangleq \{y : (x, y) \in \mathbb{S}, \exists x\}$, respectively. Similarly define $\mathbb{S}_x^{(i,j)}, \mathbb{S}_y^{(i,j)}, \overline{\mathbb{S}}_x^{(i,j)}$, and $\overline{\mathbb{S}}_y^{(i,j)}$. The ith column of $\tilde{\boldsymbol{H}}_R[k]$ and the jth row of $\tilde{\boldsymbol{H}}_T[k]$ are denoted by $\tilde{\boldsymbol{h}}_{R,i}[k]$ and $\tilde{\boldsymbol{h}}_{T,j}[k]^{\mathcal{T}}$, respectively.

Lemma 3: If Condition D1) is satisfied, then every $(i,j) \in \mathbb{S}$ is connected to every $(i',j') \in \mathbb{S}$.

Proof: If there exist $(i,j) \in \mathbb{S}$ and $(i',j') \in \mathbb{S}$ such that $(i,j) \nsim (i',j')$, then $\overline{\mathbb{S}}^{(i,j)} \neq \emptyset$ by *Definition 2*. Let $\beta_1[k]$ and $\beta_2[k]$ be different non-zero complex numbers. Then, the matrix $\boldsymbol{M}[k]$ in (16) does not change even if

- $\tilde{\boldsymbol{h}}_{R,a}[k]$ for all $a \in \mathbb{S}_x^{(i,j)}$ are replaced by $\beta_1[k]\tilde{\boldsymbol{h}}_{R,a}[k]$ and $\tilde{\boldsymbol{h}}_{T,b}[k]^{\mathcal{T}}$ for all $b \in \mathbb{S}_y^{(i,j)}$ are replaced by $(1/\beta_1[k])\tilde{\boldsymbol{h}}_{T,b}[k]^{\mathcal{T}}$, and
- $\tilde{\boldsymbol{h}}_{R,a}[k]$ for all $a \in \overline{\mathbb{S}}_x^{(i,j)}$ are replaced by $\beta_2[k]\tilde{\boldsymbol{h}}_{R,a}[k]$ and $\tilde{\boldsymbol{h}}_{T,b}[k]^{\mathcal{T}}$ for all $b \in \overline{\mathbb{S}}_y^{(i,j)}$ are replaced by $(1/\beta_2[k])\tilde{\boldsymbol{h}}_{T,b}[k]^{\mathcal{T}}$.

Note that the pairs of response matrices before and after these replacements are not equivalent under scalar ambiguity. Therefore, Condition D1) is not satisfied. $\square$

That is, if there are two pairs in $\mathbb{S}$ that are not connected to each other then Condition D1) is not satisfied.

Lemma 4: If Condition D1) is satisfied, then $\mathbb{S}_x = \{1,2,\cdots,N_R\}$ and $\mathbb{S}_y = \{1,2,\cdots,N_T\}$.

Proof: If there exists $i \in \{1,2,\cdots,N_R\}$ such that $i \notin \mathbb{S}_x$, then the matrix $\boldsymbol{M}[k]$ in (16) does not change even if $\tilde{\boldsymbol{h}}_{R,i}[k]$ is replaced by an arbitrary different vector of the same length but all the other columns of $\tilde{\boldsymbol{H}}_R[k]$ and all the rows of $\tilde{\boldsymbol{H}}_T[k]$ are not altered. Similarly, if there exists $j \in \{1,2,\cdots,N_T\}$ such that $j \notin \mathbb{S}_y$, then $\boldsymbol{M}[k]$ in (16) does not change even if $\tilde{\boldsymbol{h}}_{T,j}[k]^{\mathcal{T}}$ is replaced by an arbitrary different vector of the same length but all the other rows of $\tilde{\boldsymbol{H}}_T[k]$ and all the columns of $\tilde{\boldsymbol{H}}_R[k]$ are not altered. Note that the pairs of response matrices before and after these replacements are not equivalent under scalar ambiguity. Therefore, Condition D1) is not satisfied. $\square$

That is, if there is a Tx or an Rx port that is not used by the test channels then Condition D1) is not satisfied. The following theorem shows that the converse is also true.

Theorem 1: Condition D1) is satisfied if and only if

T1) $(i,j) \sim (i',j')$ for any $(i,j) \in \mathbb{S}$ and $(i',j') \in \mathbb{S}$, and
T2) $\mathbb{S}_x = \{1,2,\cdots,N_R\}$ and $\mathbb{S}_y = \{1,2,\cdots,N_T\}$.

Proof: The direct part is already proved in *Lemmas 3* and 4. Hence, it suffices to show the converse. Suppose that a set $\mathbb{S}$ that satisfies Conditions T1) and T2) is given. It has to be shown that all the response matrices that generate the same non-zero matrix $\boldsymbol{M}[k]$ in (16) are the form of $\left(\beta[k]\tilde{\boldsymbol{H}}_R[k], (1/\beta[k])\tilde{\boldsymbol{H}}_T[k]\right)$, where $\beta[k]$ is a complex-valued non-zero scalar. Given $\mathbb{S}$, let $\left(\tilde{\boldsymbol{U}}_1[k], \tilde{\boldsymbol{V}}_1[k]\right)$ and $\left(\tilde{\boldsymbol{U}}_2[k], \tilde{\boldsymbol{V}}_2[k]\right)$ be two pairs of response matrices that generate the same $\boldsymbol{M}[k]$. Then, by (16), the ith columns $\tilde{\boldsymbol{u}}_{1,i}[k]$ and $\tilde{\boldsymbol{u}}_{2,i}[k]$ of $\tilde{\boldsymbol{U}}_1[k]$ and $\tilde{\boldsymbol{U}}_2[k]$ respectively, and the jth rows $\tilde{\boldsymbol{v}}_{1,j}[k]^{\mathcal{T}}$ and $\tilde{\boldsymbol{v}}_{2,j}[k]^{\mathcal{T}}$ of $\tilde{\boldsymbol{V}}_1[k]$ and $\tilde{\boldsymbol{V}}_2[k]$, respectively, must satisfy

$$\tilde{\boldsymbol{u}}_{1,i}[k]\tilde{\boldsymbol{v}}_{1,j}[k]^{\mathcal{T}} = \tilde{\boldsymbol{u}}_{2,i}[k]\tilde{\boldsymbol{v}}_{2,j}[k]^{\mathcal{T}}, \tag{17}$$

for each $(i,j) \in \mathbb{S}$. Thus, there exists non-zero $\beta^{(i,j)}[k]$ such that

$$\tilde{\boldsymbol{u}}_{1,i}[k] = \beta^{(i,j)}[k]\tilde{\boldsymbol{u}}_{2,i}[k] \tag{18a}$$

and

$$\tilde{\boldsymbol{v}}_{1,j}[k] = (1/\beta^{(i,j)}[k])\tilde{\boldsymbol{v}}_{2,j}[k]. \tag{18b}$$

For connected pairs $(i,j) \in \mathbb{S}$ and $(i',j') \in \mathbb{S}$, there exists a sequence $(a_p,b_p)_p$ defined in *Definition 2*. Then, $\beta^{(a_p,b_p)}[k]$ must be the same for every element (a_p,b_p) in the sequence. This is because, otherwise, there exist distinct elements (a_n,b_n) and (a_{n+1},b_{n+1}) such that $\beta^{(a_n,b_n)}[k] \neq \beta^{(a_{n+1},b_{n+1})}[k]$, which implies

- if $a_n = a_{n+1}$, at least one of the two equalities $\tilde{\boldsymbol{u}}_{1,a_n}[k] = \beta^{(a_n,b_n)}[k]\tilde{\boldsymbol{u}}_{2,a_n}[k]$ and $\tilde{\boldsymbol{u}}_{1,a_{n+1}}[k] = \beta^{(a_{n+1},b_{n+1})}[k]\tilde{\boldsymbol{u}}_{2,a_{n+1}}[k]$ cannot be satisfied, and
- if $b_n = b_{n+1}$, at least one of the two equalities $\tilde{\boldsymbol{v}}_{1,b_n}[k] = (1/\beta^{(a_n,b_n)}[k])\tilde{\boldsymbol{v}}_{2,b_n}[k]$ and $\tilde{\boldsymbol{v}}_{1,b_{n+1}}[k] = (1/\beta^{(a_{n+1},b_{n+1})}[k])\tilde{\boldsymbol{v}}_{2,b_{n+1}}[k]$ cannot be satisfied.

This contradicts to (18). Since all the elements of $\mathbb{S}$ are connected to each other by Condition T1), the scalars $\beta^{(i,j)}[k]$ for all $(i,j) \in \mathbb{S}$ are the same. Note that every column of $\tilde{\boldsymbol{U}}_1[k]$ and $\tilde{\boldsymbol{U}}_2[k]$, every row of $\tilde{\boldsymbol{V}}_1[k]$ and $\tilde{\boldsymbol{V}}_2[k]$ is determined because every column index and every row index is included in $\mathbb{S}_x$ and $\mathbb{S}_y$, respectively, by Condition T2). Therefore, all the response matrices that generate the given $\boldsymbol{M}[k]$ are equivalent under the scalar ambiguity and thus Condition D1) is satisfied. $\square$

As the number L of observations in (6a) tends to infinity, $\tilde{\boldsymbol{Z}}[k]$ converges to its mean value almost surely by the law of large numbers. Hence, given $\tilde{\boldsymbol{h}}_R[k]$ and $\tilde{\boldsymbol{h}}_T[k]$, the LS estimation problem becomes solving the bi-linear equation

$$\boldsymbol{W} \odot \tilde{\boldsymbol{h}}_R[k]\tilde{\boldsymbol{h}}_T[k]^{\mathcal{T}} = \boldsymbol{W} \odot \check{\boldsymbol{h}}_R[k]\check{\boldsymbol{h}}_T[k]^{\mathcal{T}}. \tag{19}$$

It is already shown that, if Condition D1) is satisfied by $\boldsymbol{W}$, the solution pair $(\check{\boldsymbol{H}}_R[k], \check{\boldsymbol{H}}_T[k])$ is equivalent to the pair $(\tilde{\boldsymbol{H}}_R[k], \tilde{\boldsymbol{H}}_T[k])$ under scalar ambiguity. Thus, if Condition D1) is satisfied, then Condition D2) is also satisfied.

B. Minimum Number of B2B Connections for Identifiability

Consider an exemplary set of test channels, which makes the system identifiable.

Example 1: The set of test channels

$$\mathbb{S}_\Gamma \triangleq \{(1,1),(2,1),\cdots,(N_R,1),$$
$$(1,2),(1,3),\cdots,(1,N_T)\}, \tag{20a}$$

corresponding to the N_R-by-N_T blockwise weight matrix

$$\boldsymbol{B}_\Gamma \triangleq \begin{bmatrix} 1 & 1 & \cdots & 1 \\ 1 & 0 & \cdots & 0 \\ \vdots & \vdots & \vdots & \vdots \\ 1 & 0 & \cdots & 0 \\ 1 & 0 & \cdots & 0 \end{bmatrix} \tag{20b}$$

makes the system identifiable.

Notice that this example has $|\mathbb{S}_\Gamma| = N_T + N_R - 1$. Since $|\mathbb{S}|$ is the number of B2B connections, we are interested in finding the sets that achieve the minimum value of $|\mathbb{S}|$ when $\mathbb{S}$ makes the system identifiable. The next theorem provides the achievable lower bound on $|\mathbb{S}|$.

Theorem 2: If the system is identifiable, then the minimum cardinality of $\mathbb{S}$ is $N_T + N_R - 1$.

Proof: If the system is identifiable, then there exists a length-Q sequence $(c_q, d_q)_q$ for $q = 1, 2, \cdots, Q < \infty$ such that

- $\{(c_q, d_q) : q = 1, 2, \cdots, Q\} = \mathbb{S}$,
- $c_{q+1} = c_q$ or $d_{q+1} = d_q$ for all $q = 1, 2, \cdots, Q - 1$.

Such a sequence can be constructed as follows. *Lemma 3* implies that a sequence in *Definition 2* exists for all $(i, j) \in \mathbb{S}$ and $(i', j') \in \mathbb{S}$ pair. Thus, a sequence $(c_q, d_q)_q$ can be obtained by concatenating $|\mathbb{S}| - 1$ sequences that connect two consecutive pairs starting from (i_1, j_1) and (i_2, j_2) to $(i_{|\mathbb{S}|-1}, j_{|\mathbb{S}|-1})$ and $(i_{|\mathbb{S}|}, j_{|\mathbb{S}|})$, where (i_1, j_1) to $(i_{|\mathbb{S}|}, j_{|\mathbb{S}|})$ are distinct elements of $\mathbb{S}$. Since $c_{q+1} = c_q$ or $d_{q+1} = d_q$ for all $q = 1, 2, \cdots, Q - 1$, and $\{c_1, c_2, \cdots, c_Q\} = \mathbb{S}_x$ and $\{d_1, d_2, \cdots, d_Q\} = \mathbb{S}_y$, the cardinality of the set $\{(c_q, d_q) : q = 1, 2, \cdots, Q\}$ must be greater than or equal to $|\mathbb{S}_x| + |\mathbb{S}_y| - 1$. Thus, $|\mathbb{S}| \geq |\mathbb{S}_x| + |\mathbb{S}_y| - 1$. This gives the lower bound as $|\mathbb{S}| \geq N_T + N_R - 1$ because $|\mathbb{S}_x| + |\mathbb{S}_y|$ is $N_T + N_R$ by *Lemma 4*. Recall that $\mathbb{S}_\vdash$ defined in *Example 1* is such a set. Therefore, the conclusion follows. □

After the set $\mathbb{S}$ of test channels is chosen to satisfy the system identifiability, the order to perform the $|\mathbb{S}|$ test channel measurements also needs to be determined. Define a unit *labor* in the test channel measurement as a connection or a disconnection of a terminal of a test channel with an RF port. Then, among $|\mathbb{S}|!$ different orderings of the test channel measurements, an ordering may have less number of labors than another ordering. Obviously, the upper bound on the number of labors is $4|\mathbb{S}|$, where and in what follows it is assumed that initially no terminal is connected to an RF port and that finally the terminals are disconnected with RF ports. The next theorem provides the achievable lower bound on the number of labors.

Theorem 3: If $\mathbb{S}$ makes the system identifiable, then the minimum number of labors in the test channel measurements is $2(N_T + N_R)$.

Proof: If $\mathbb{S}$ exists such that it makes the system identifiable, $|\mathbb{S}| = N_T + N_R - 1$, and every consecutive pair (i, j) and (i', j') in the ordering satisfies $i = i'$ or $j = j'$, then the number of labors is minimized and given by $2(N_T + N_R)$. Recall that $\mathbb{S}_\vdash$ defined in *Example 1* is such a set when the elements are ordered as $(N_R, 1), (N_R - 1, 1), \cdots, (1, 1), (1, 2), \cdots, (1, N_T)$. Therefore, the conclusion follows. □

Our objective is to find an optimal set of test channels that not only makes the system identifiable with $|\mathbb{S}| = N_T + N_R - 1$ but also achieves the minimum number of labors. However, every set $\mathbb{S}$ that makes the system identifiable with $|\mathbb{S}| = N_T + N_R - 1$ does not in general have an ordering that achieves the above lower bound. This is because finding an ordering that achieves the lower bound is equivalent to finding a Hamilton path in a graph. Since every graph does not necessarily have a Hamilton path [41], the lower bound may not be achieved.

Example 2: The set of test channels

$$\mathbb{S}_\neg \triangleq \{(1, 1), (1, 2), \cdots, (1, N_T), \\ (2, N_T), \cdots, (N_R, N_T)\}, \tag{21a}$$

corresponding to the N_R-by-N_T blockwise weight matrix

$$\boldsymbol{B}_\neg \triangleq \begin{bmatrix} 1 & \cdots & 1 & 1 \\ 0 & \cdots & 0 & 1 \\ \vdots & \vdots & \vdots & \vdots \\ 0 & \cdots & 0 & 1 \\ 0 & \cdots & 0 & 1 \end{bmatrix} \tag{21b}$$

makes the system identifiable. Moreover, the ordering $(1, 1), (1, 2), \cdots, (1, N_T), (2, N_T), \cdots, (N_R, N_T)$ minimizes the number of labors.

The set $\mathbb{S}_\neg$ of test channels is optimal in that it achieves the minimum number of labors. Similarly, it can be shown that the set $\mathbb{S}_\vdash$ in *Example 1* is also optimal. Other variants such as $\mathbb{S}_\lrcorner$ and $\mathbb{S}_\llcorner$ can be similarly defined and shown to be optimal. Thus, $\mathbb{S}_\vdash$ and its variants are good choices of $\mathbb{S}$.

In the following subsection, a numerical solution along with an initialization scheme is provided to the LS estimation problem in (15).

C. Solutions to System Identification Problem

In general, no analytical solution is known to weighted rank-one approximation problems [39, Sec. 2.1]. For example, our problem in (15) has no analytical solution when $\boldsymbol{W} = \boldsymbol{W}_\vdash$ though it makes the system identifiable. Of course, analytical solutions are known for some special weight matrices such as rank-one matrices [39, Sec. 2.1]. Recall that the all-one weight matrix $\boldsymbol{W} = \mathbf{1}_{N_R^2 \times N_T^2} = \mathbf{1}_{N_R^2} \mathbf{1}_{N_T^2}^{\mathcal{T}}$ is of rank one and leads to constant multiples of the left and right singular vectors of the measurement matrix as analytical solutions [17].

To find solutions to general weighted rank-one approximation problems, numerical methods such as the ACS algorithm have been used [39], [42], [43]. The ACS algorithm is applicable to a problem with a biconvex objective function $f : X \times Y \to \mathbb{R}$, where $f(x, y)$ is convex in y for a fixed $x \in X$ and $f(x, y)$ is convex in x for a fixed $y \in Y$. This numerical method alternates the minimization of the objective function with respect to a parameter set with the other parameter set being fixed. Note that our weighted rank-one approximation problem has its objective function biconvex in $\tilde{\boldsymbol{u}}[k]$ and $\tilde{\boldsymbol{v}}[k]$.

Theorem 4: The ACS algorithm to numerically solve the system identification problem in (15) is given as follows.

Algorithm: ACS algorithm to estimate the response matrices of the MIMO channel sounder

Input: $\tilde{\boldsymbol{Z}}^{(i,j)}[k], \tilde{\boldsymbol{G}}^{(i,j)}[k]$, where $(i, j) \in \mathbb{S}$
Output: $\check{\boldsymbol{H}}_R[k], \check{\boldsymbol{H}}_T[k]$

1: Choose $\tilde{\boldsymbol{U}}^{(0)}[k]$ and set $n = 0$;
2: **repeat**
3:      $n \leftarrow n + 1$;
4:      compute $\tilde{\boldsymbol{V}}^{(n)}[k] = \check{\boldsymbol{H}}_T(\tilde{\boldsymbol{U}}^{(n-1)}[k])$;
5:      compute $\tilde{\boldsymbol{U}}^{(n)}[k] = \check{\boldsymbol{H}}_R(\tilde{\boldsymbol{V}}^{(n)}[k])$;
6: **until** $\frac{\|\tilde{\boldsymbol{U}}^{(n)}[k] - \tilde{\boldsymbol{U}}^{(n-1)}[k]\|_F^2 + \|\tilde{\boldsymbol{V}}^{(n)}[k] - \tilde{\boldsymbol{V}}^{(n-1)}[k]\|_F^2}{\|\tilde{\boldsymbol{U}}^{(n)}[k]\|_F^2 + \|\tilde{\boldsymbol{V}}^{(n)}[k]\|_F^2} < \epsilon$
7: **return** $\check{\boldsymbol{H}}_R[k] = \tilde{\boldsymbol{U}}^{(n)}[k], \check{\boldsymbol{H}}_T[k] = \tilde{\boldsymbol{V}}^{(n)}[k]$;

where $\mathbb{S}$ is chosen to make the system identifiable, and $\tilde{\boldsymbol{G}}^{(i,j)}[k]$ and the update functions are defined by

$$\tilde{\boldsymbol{G}}^{(i,j)}[k] \triangleq T_s^3 \tilde{x}[k]\tilde{g}[k]\boldsymbol{e}_i\boldsymbol{e}_j^{\mathcal{T}}, \tag{22a}$$

$$\check{\boldsymbol{H}}_T(\tilde{\boldsymbol{U}}[k]) \triangleq$$
$$\left(\sum_{(i,j)\in\mathbb{S}} \tilde{\boldsymbol{G}}^{(i,j)}[k]^{\mathcal{H}}\tilde{\boldsymbol{U}}[k]^{\mathcal{H}}\tilde{\boldsymbol{U}}[k]\tilde{\boldsymbol{G}}^{(i,j)}[k] \right)^{-1}$$
$$\left(\sum_{(i,j)\in\mathbb{S}} \tilde{\boldsymbol{G}}^{(i,j)}[k]^{\mathcal{H}}\tilde{\boldsymbol{U}}[k]^{\mathcal{H}}\tilde{\boldsymbol{Z}}^{(i,j)}[k] \right), \text{ and} \tag{22b}$$

$$\check{\boldsymbol{H}}_R(\tilde{\boldsymbol{V}}[k]) \triangleq$$
$$\left(\sum_{(i,j)\in\mathbb{S}} \tilde{\boldsymbol{Z}}^{(i,j)}[k]\tilde{\boldsymbol{V}}[k]^{\mathcal{H}}\tilde{\boldsymbol{G}}^{(i,j)}[k]^{\mathcal{H}} \right)$$
$$\left(\sum_{(i,j)\in\mathbb{S}} \tilde{\boldsymbol{G}}^{(i,j)}[k]\tilde{\boldsymbol{V}}[k]\tilde{\boldsymbol{V}}[k]^{\mathcal{H}}\tilde{\boldsymbol{G}}^{(i,j)}[k]^{\mathcal{H}} \right)^{-1}. \tag{22c}$$

Proof: By finding the gradient of the objective function with respect to $\tilde{\boldsymbol{U}}[k]$ and setting it to zero to satisfy the first-order necessary condition, we have the update function for $\check{\boldsymbol{H}}_T[k]$ as (22b). Note that the matrix inverse in (22b) is well defined. This is because the argument of the inverse operation is the summation of $T_s^3 \tilde{x}[k]\tilde{g}[k]\|\tilde{\boldsymbol{U}}[k]\boldsymbol{e}_i\|^2\boldsymbol{e}_j\boldsymbol{e}_j^{\mathcal{T}}$, and the summation is performed for all $j \in \{1, 2, \cdots, N_T\} = \mathbb{S}_y$ due to *Theorem 1*, which makes the argument matrix a diagonal matrix with non-zero diagonal entries. Hence, the nth iterate $\tilde{\boldsymbol{V}}^{(n)}[k]$ is given by line 4. Similarly, we have the update function for $\check{\boldsymbol{H}}_R[k]$ as (22c), where the matrix inverse is also well defined. Hence, the nth estimate $\tilde{\boldsymbol{U}}^{(n)}[k]$ is given by line 5. Detailed derivations of the update functions can be found in Appendix. If the normalized squared difference is employed for the stopping criterion, then we have line 6 for $n \geq 2$. Therefore, the conclusion follows. $\square$

Here, we have chosen to update the estimate for $\tilde{\boldsymbol{H}}_T[k]$ first, so that an initialization only for $\tilde{\boldsymbol{H}}_R[k]$ is needed as line 1. The other way is also possible by choosing $\tilde{\boldsymbol{V}}^{(0)}[k]$ and updating the estimate for $\tilde{\boldsymbol{H}}_R[k]$ first.

Since the squared error in (15) with its biconvex structure monotonically decreases during the iterative minimization, the estimate converges to a stationary point of the objective function [43, Sec. 4.2.1]. A proper initialization of the ACS algorithm is very crucial because, otherwise, the estimate may converge to a local minimizer that is much inferior to the global minimizer. A simplest approach is to randomly initialize. Another simplest approach is to have an identity matrix as the initial estimate $\tilde{\boldsymbol{U}}^{(0)}[k]$, which ignores both the frequency selectivity and the crosstalk inside the Rx. It turns out that both the random initialization and the identity matrix initialization, which can be employed for any set $\mathbb{S}$ that makes the system identifiable, do not perform well as it will be shown in numerical results. Interestingly, for the set $\mathbb{S}_\vdash$ of test channels and its variants $\mathbb{S}_\neg, \mathbb{S}_\lrcorner$ and $\mathbb{S}_\llcorner$, there is a better approach to initialization.

Proposition 2: Given $\boldsymbol{W}_\vdash$ and $\tilde{\boldsymbol{Z}}[k]$, an initial estimate

$$\tilde{\boldsymbol{u}}^{(0)}[k] = \tilde{\boldsymbol{Z}}[k]\boldsymbol{e}_1 \tag{23}$$

converges to a scalar-multiple of the true value $\tilde{\boldsymbol{h}}_R[k]$ as the number of observations tends to infinity.

Proof: As the number L of observations in (6a) tends to infinity, $\tilde{\boldsymbol{Z}}[k]$ converges to its mean almost surely by the law of large numbers. Hence, $\tilde{\boldsymbol{Z}}[k]\boldsymbol{e}_1$ converges to $T_s^3\tilde{x}[k]\tilde{g}[k](\boldsymbol{e}_1^{\mathcal{T}}\tilde{\boldsymbol{H}}_T[k]\boldsymbol{e}_1)\tilde{\boldsymbol{h}}_R[k]$, which is a scalar-multiple of $\tilde{\boldsymbol{h}}_R[k]$. Therefore, the conclusion follows. $\square$

This initial estimate that utilizes the first column of $\tilde{\boldsymbol{Z}}[k]$ performs well as shown in numerical results. It turns out that an estimate

$$\tilde{\boldsymbol{v}}^{(0)}[k] = \tilde{\boldsymbol{Z}}[k]^{\mathcal{T}}\boldsymbol{e}_1 \tag{24}$$

that utilizes the first row of $\tilde{\boldsymbol{Z}}[k]$ performs well as an initial estimate of $\tilde{\boldsymbol{h}}_T[k]$, when we choose to update the estimate for $\tilde{\boldsymbol{H}}_R[k]$ first in the ACS algorithm. For the weight matrices $\boldsymbol{W}_\neg, \boldsymbol{W}_\lrcorner$, and $\boldsymbol{W}_\llcorner$, initial estimates can be found in a similar way.

Motivated by these initial estimates in (23) and (24), we propose an analytical approximate solution to the identification problem as

$$\check{\boldsymbol{h}}_R[k] = \tilde{\boldsymbol{Z}}[k]\boldsymbol{e}_1, \text{ and} \tag{25a}$$

$$\check{\boldsymbol{h}}_T[k] = \frac{1}{T_s^3\tilde{x}[k]\tilde{g}[k](\boldsymbol{e}_1^{\mathcal{T}}\tilde{\boldsymbol{Z}}[k]\boldsymbol{e}_1)}\tilde{\boldsymbol{Z}}[k]^{\mathcal{T}}\boldsymbol{e}_1. \tag{25b}$$

The fraction pre-multiplied to (24) to obtain (25b) is to make the product $\check{\boldsymbol{h}}_R[k]\check{\boldsymbol{h}}_T[k]^{\mathcal{T}}$ converge to $\tilde{\boldsymbol{h}}_R[k]\tilde{\boldsymbol{h}}_T[k]^{\mathcal{T}}$ as the number of observations tends to infinity.

In the next section, we provide discussions and numerical results.

V. DISCUSSIONS AND SIMULATION RESULTS

In this section, we first briefly discuss how to estimate the channel by calibrating field measurement data. We also discuss complexity issues. Then, we provide simulation results, which verify the effectiveness of the proposed system model and efficient system identification procedure exploiting less B2B measurements.

A. Channel Estimation Based on Field Measurement Data

It is assumed that the TDM-based signal and system model described in (2b) and Fig. 1 is also employed for field measurements. Hence, the sampled output can be rearranged into a sequence of N_R-by-N_T matrices similar to $(\boldsymbol{Z}^{(i,j)}[m])_m$ in (6b). For convenience, we denote the rearranged output by $\boldsymbol{Z}^{(0,0)}[m]$. Then, the input-output relation in the FD can be written by

$$\tilde{\boldsymbol{Z}}^{(0,0)}[k] = T_s^3\left(\tilde{\boldsymbol{H}}_R[k]\boldsymbol{C}_R\tilde{\boldsymbol{H}}[k]\boldsymbol{C}_T\tilde{\boldsymbol{H}}_T[k]\right)\tilde{x}[k]$$
$$+ \tilde{\boldsymbol{N}}^{(0,0)}[k], \tag{26}$$

where $\tilde{\boldsymbol{H}}[k]$ is the DTFT of $\boldsymbol{H}[m] \triangleq \boldsymbol{H}(mT_s)$ evaluated at $f = k/(MN)$, and $\tilde{\boldsymbol{N}}^{(0,0)}[k]$ is the noise component in $\tilde{\boldsymbol{Z}}^{(0,0)}[k]$.

Given the estimate $(\check{\boldsymbol{H}}_R[k], \check{\boldsymbol{H}}_T[k])_k$ of the FD Rx-Tx response matrices, let $\check{\boldsymbol{E}}^{(0,0)}[k]$ be the model error function defined by

$$\check{\boldsymbol{E}}^{(0,0)}[k] \triangleq \tilde{\boldsymbol{Z}}^{(0,0)}[k] - T_s^3\tilde{x}[k]\check{\boldsymbol{H}}_R[k]\boldsymbol{C}_R\tilde{\boldsymbol{F}}[k]\boldsymbol{C}_T\check{\boldsymbol{H}}_T[k] \tag{27a}$$

Table I
COMPLEXITIES OF CONVENTIONAL AND PROPOSED METHODS

complexities \ methods	conventional [17]	conventional [19]	proposed
experiment	$\mathcal{O}(N_T N_R)$	$\mathcal{O}(N_T + N_R)$	$\mathcal{O}(N_T + N_R)$
$(\check{\boldsymbol{H}}_R[k], \check{\boldsymbol{H}}_T[k])_k$ estimation	$\mathcal{O}(N_T^2 N_R^2 MN)$	$\mathcal{O}((N_T + N_R)MN)$	$\mathcal{O}((N_T^2 N_R + N_T N_R^2)MN)$
$(\check{\boldsymbol{H}}[k])_k$ estimation	$\mathcal{O}((N_T^p + N_R^p)MN)$, with $2 < p \leq 3$		

and formulate the LS channel estimation problem as

$$\check{\boldsymbol{H}}[k] \triangleq \underset{\bar{\boldsymbol{F}}[k]}{\operatorname{argmin}} \left\| \tilde{\boldsymbol{E}}^{(0,0)}[k] \right\|_F^2, \tag{27b}$$

where $\check{\boldsymbol{H}}[k]$ is the estimate of $\tilde{\boldsymbol{H}}[k]$. Then, the estimate of the FD channel matrix can be found as

$$\check{\boldsymbol{H}}[k] \triangleq \frac{1}{T_s^3 \tilde{x}[k]} \boldsymbol{C}_R^{-1} \check{\boldsymbol{H}}_R^{-1}[k] \tilde{\boldsymbol{Z}}^{(0,0)}[k] \check{\boldsymbol{H}}_T^{-1}[k] \boldsymbol{C}_T^{-1}, \tag{28}$$

where it is assumed that all the matrix inverses in (28) exist. Note that the scalar ambiguity in the estimate $(\check{\boldsymbol{H}}_R[k], \check{\boldsymbol{H}}_T[k])_k$ does not affect the channel estimate.

An FDM or CDM-based sounding signal can also be transmitted for the field measurements. Then, an LS channel estimation problem can be formulated in the FD and solved similarly to (27) and (28) by using the estimate of $(\tilde{\boldsymbol{H}}_R[k], \tilde{\boldsymbol{H}}_T[k])_k$.

B. Complexities

There are three complexities to be compared among the method proposed in this paper and the conventional methods in [17] and [19]. The first is the experiment complexity that is the number of labors defined in Section IV-B. Both the proposed method and the conventional method in [19] require $N_T + N_R - 1$ test channels and $\mathcal{O}(N_T + N_R)$ labors, while the conventional method in [17] needs $N_T N_R$ test channels and $\mathcal{O}(N_T N_R)$ labors.

The second is the identification complexity that is the number of complex multiplications in estimating the response matrices from the B2B measurements. The conventional method in [17] has the identification complexity of $\mathcal{O}(N_T^2 N_R^2 MN)$, which comes from the rank-one approximation [46, Section 2.1] to $\tilde{\boldsymbol{Z}}[k]$. The other conventional method in [19] has the identification complexity of $\mathcal{O}((N_T + N_R)MN)$, which comes from $N_T + N_R - 1$ divisions to obtain the diagonal response matrices. In the proposed method, the matrix multiplications in the update functions (22b) and (22c) are dominant in the identification complexity, which is $\mathcal{O}((N_T^2 N_R + N_T N_R^2)MN)$ because the arguments of matrix inversion operations in update functions are diagonal matrices.

The third complexity is the calibration complexity that is the number of complex multiplications in estimating the channel matrix from the field measurement data. As shown in (28), the field measurement data $\tilde{\boldsymbol{Z}}^{(0,0)}$ is pre- and post-multiplied by the inverses of the response matrices. In the proposed method and the conventional method in [17], this can be implemented by solving two systems of linear equations, which requires the computational complexity of $\mathcal{O}((N_T^p + N_R^p)MN)$, where $2 < p \leq 3$ depends on the algorithm used [47]. In the

conventional method in [19], this requires the computational complexity only of $\mathcal{O}((N_T N_R)MN)$ because it is assumed that the response matrices are diagonal. However, all three methods commonly need the pre- and post-multiplications of the inverses of the antenna coupling matrices, which leads to the computational complexity of $\mathcal{O}((N_T^p + N_R^p)MN)$. Hence, all three methods have the calibration complexity of $\mathcal{O}((N_T^p + N_R^p)MN)$ in estimating the channel matrix. All the complexities discussed above are summarized in Table I.

C. Simulation Results

Throughout this subsection, the Tx and Rx response matrices are assumed to be in the form of $\boldsymbol{H}_T(t) = \boldsymbol{H}_T h_T(t)$ and $\boldsymbol{H}_R(t) = \boldsymbol{H}_R h_R(t)$. For $h_T(t)$ and $h_R(t)$, the estimates of $[\boldsymbol{H}_T(t)]_{1,1}$ and $[\boldsymbol{H}_R(t)]_{2,2}$ are employed that are obtained from the experiments conducted in [17]. For $\boldsymbol{H}_T$ and $\boldsymbol{H}_R$, a uniform crosstalk model parameterized by a single power level is employed, where $|[\boldsymbol{H}_T]_{i,j}| = |[\boldsymbol{H}_R]_{i,j}| = 1$ for $i = j$ but $|[\boldsymbol{H}_T]_{i,j}| = |[\boldsymbol{H}_R]_{i,j}| = \sqrt{\gamma}$ for $i \neq j$ with independent and identically generated random phase for every entry. This model well separates the effects of the frequency selectivity and the crosstalk, and is employed for simulation purpose.

It is often modeled that the power of linear crosstalk decrease as the distance between RF paths increases [36], [37]. In this sense, our model looks simplistic. However, as already mentioned in Section III-B, our problem formulation and solution can also be applied to a semi-switched and fully-switched MIMO channel sounders with a periodic test signal. Interestingly, some commercial RF switches such as the 1-by-6 RF switch in [44] actually exhibit almost uniform crosstalk power among RF paths. Experimental data in [17] also confirms that a switched sounder may have nearly uniform level of crosstalk.

For the antenna coupling matrices, it is modeled that $\boldsymbol{C}_T$ and $\boldsymbol{C}_R$ are Toeplitz symmetrical matrices with $[\boldsymbol{C}_T]_{i,j} = [\boldsymbol{C}_R]_{i,j} = \delta^{|i-j|}$ with $\delta = 0.01$. The Vienna channel simulator that implements the spatial channel model (SCM) described in [45] is used to generate the channel impulse response $\boldsymbol{H}(t)$ in the urban micro-cell scenario. For the B2B measurements, $\boldsymbol{W} = \boldsymbol{W}_\ulcorner$ is assumed as the weight matrix. Both for the B2B and field measurements, the TDM-based sounding signal in (3) is assumed to be transmitted and the oversampling factor in the Rx is $M = 2$, where $(b[n])_n$ is an m-sequence with period $N = 1023$ and $p(t)$ is the square-root raised cosine (SRRC) pulse with roll-off factor $\alpha = 0.22$ and chip rate $1/T_c = 100$ MHz.

Fig. 3 shows how different initialization schemes affect the rate of convergence of the ACS algorithm in estimating the response matrices with $N_T = N_R = 4$. At each frequency
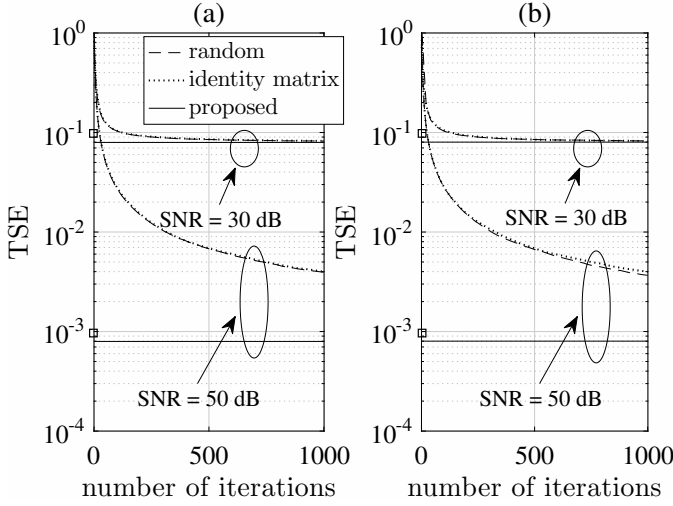
Fig. 3. TSE as a function of the number of iterations of the ACS algorithm applied to $N_T = N_R = 4$ with random and identity matrix initializations, and proposed initialization in (23): (a) $\gamma = -45$ dB, (b) $\gamma = -25$ dB.
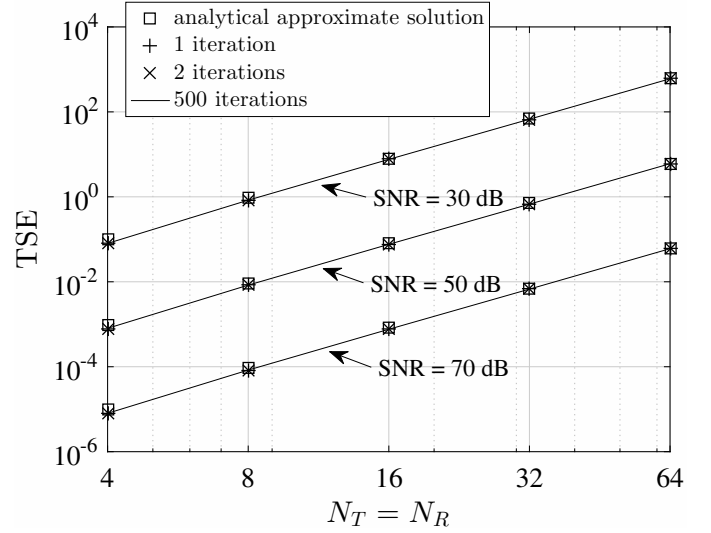

Fig. 4. TSE as a function of $N_T = N_R$ obtained by using the analytical approximate solution in (25) and the ACS algorithm with proposed initialization in (23). $\gamma = -25$ dB.

bin k, the ACS algorithm is used to minimize the objective function in (15) with the random initialization, the identity matrix initialization, and the proposed initialization in (23). The total squared error (TSE) defined as the sum of the objective function values evaluated at all k of interest is shown as a function of the number of iterations, after being averaged over 10^4 realizations of $(\boldsymbol{H}_R, \boldsymbol{H}_T)$. Here, we do not terminate the algorithm to see the convergence characteristics. The TSE of the proposed scheme at the 0th iteration is that of the analytical approximate solution in (25), where the same estimate for $\tilde{\boldsymbol{h}}_R[k]$ is shared as the proposed initialization in (23). The response matrices are assumed to have the crosstalk level γ chosen to be -45 dB and -25 dB to simulate relatively small and large crosstalk environments. The B2B measurement SNR is 30 and 50 dB to simulate a high and moderate noise environment in the B2B measurements, respectively. It can be seen that the proposed initialization scheme in (23) has a much faster convergence than the other initialization schemes that perform almost the same. The markers at the 0th iteration show that the performance of the analytical approximate solution in (25) is even better than that of the other initialization schemes.

Fig. 4 investigates the performance of the analytical approximate solution in (25) and that of the ACS algorithm with proposed initialization in (23) as a function of the number of ports when $N_T = N_R = 4, 8, 16, 32,$ and 64. The B2B measurement SNR is 30, 50, and 70 dB to simulate a high, moderate, and low noise environment, respectively. The TSE of the analytical approximate solution, and the TSE after $1, 2,$ and 500 iterations of the ACS algorithm are compared. It can be seen that, only a couple of iterations are enough to obtain a final estimate, e.g., line 6 of the ACS algorithm can be replaced by 'until $n = 2$.'

Fig. 5 shows the impact of the number of B2B connections on the calibration performance. To find the estimate of $(\tilde{\boldsymbol{H}}_R[k], \tilde{\boldsymbol{H}}_T[k])$, the proposed method has $\boldsymbol{W}^{\vdash}$ and two iterations of the ACS algorithm with (23) as the initial estimate. For convenience, starting with $\boldsymbol{B}^{\vdash}$ having $N_T = N_R = 64$, we
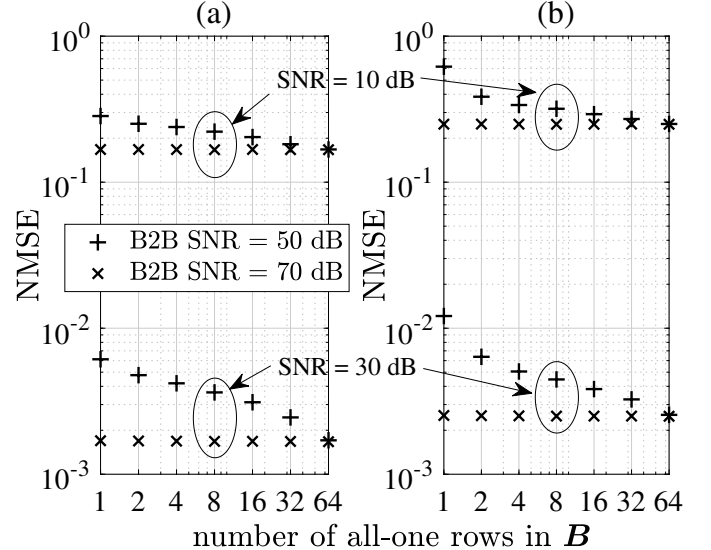
Fig. 5. NMSE as a function of the number of all-one rows in blockwise weight matrix $\boldsymbol{B}$: (a) $\gamma = -45$ dB, (b) $\gamma = -25$ dB.

increase the number of all-one rows up to 64 by replacing the first 2^k rows to all-one rows, for $k = 1, 2, \cdots, 6$. Since these different weight matrices lead to different performance metrics in the LS system identifications, we use the channel estimation error in the field measurements as a common performance metric instead of the TSE. Specifically, the normalized mean-squared error (NMSE) in the FD defined by

$$\text{NMSE} \triangleq \frac{\sum_k \left\| \check{\boldsymbol{H}}[k] - \tilde{\boldsymbol{H}}[k] \right\|_F^2}{\sum_k \left\| \tilde{\boldsymbol{H}}[k] \right\|_F^2} \qquad (29)$$

is shown as a function of the number of all-one rows, after being averaged over 10^4 realizations of $(\boldsymbol{H}_R, \boldsymbol{H}(t), \boldsymbol{H}_T)$. All the channel estimations are performed as (28). It can be seen that the NMSE as a decreasing function of the number of B2B connections exhibits a noticeable variation when the B2B SNR
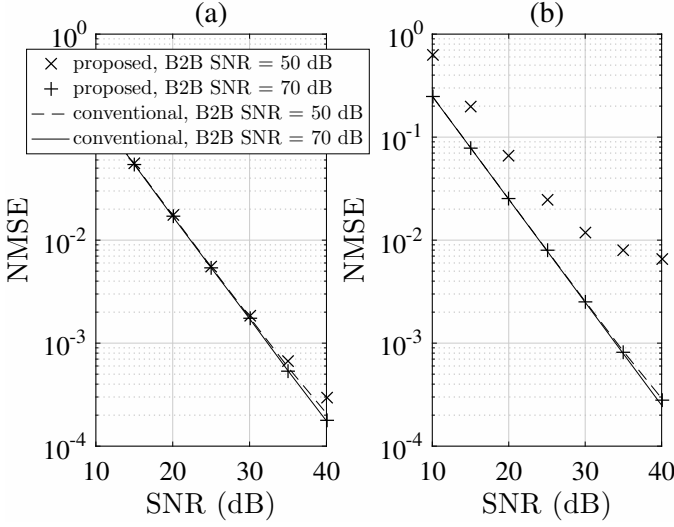
Fig. 6. NMSE as a function of field measurement SNR. The proposed method with $\boldsymbol{W} = \boldsymbol{W}_{\vdash}$ has the number of B2B connections $N_T + N_R - 1$ but the conventional method in [17] with $\boldsymbol{W} = \mathbf{1}_{N_R^2 \times N_T^2}$ has the number of B2B connections $N_T N_R$: (a) $N_T = N_R = 4$, (b) $N_T = N_R = 64$
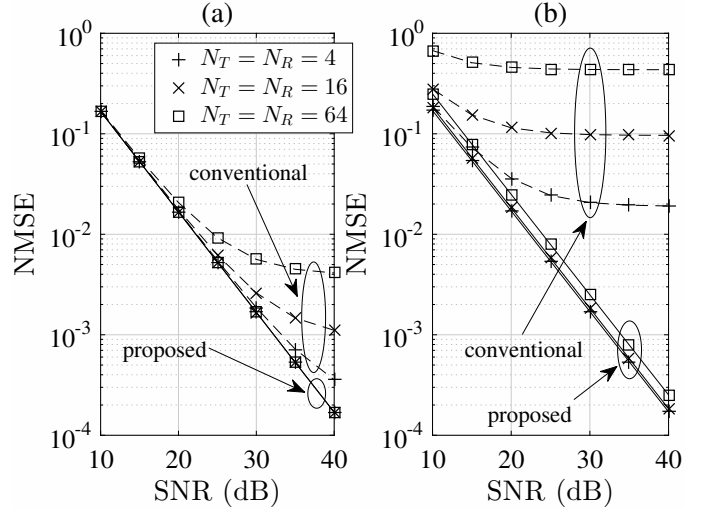

Fig. 7. NMSE as a function of field measurement SNR. Both proposed method and conventional method in [19] need $N_T + N_R - 1$ B2B connections but the conventional method ignores the crosstalk. B2B measurement SNR = 70 dB and $N_T = N_R = 4, 16$, and 64: (a) $\gamma = -45$ dB, (b) $\gamma = -25$ dB.

is relatively low, e.g. 50 dB. However, for both crosstalk level $\gamma = -45$ and -25 dB and for both field measurement SNR 10 and 30 dB, there is no noticeable variation in the NMSE when the B2B SNR is relative high, e.g. 70 dB, which is the case in most of the practical situations. In other words, $\boldsymbol{B} = \mathbf{1}_{N_R \times N_T}$ can be replaced by $\boldsymbol{B}_{\vdash}$.

Fig. 6 compares the performance of the proposed system identification method and that of a conventional method in [17]. The proposed method is the same as Fig. 5. On the other hand, the conventional method has $\boldsymbol{W} = \mathbf{1}_{N_R^2 \times N_T^2}$ and performs the rank-one approximation to $\tilde{\boldsymbol{Z}}[k]$. Since two different weight matrices are used, we again show the NMSE now as a function of the field measurement SNR, after being averaged over 10^4 realizations of $(\boldsymbol{H}_R, \boldsymbol{H}(t), \boldsymbol{H}_T)$. The NMSE is compared for $N_T = N_R = 4$ and $N_T = N_R = 64$ both with $\gamma = -25$ dB. It can be seen in Fig. 6-(a) that, with the small number of antennas $N_T = N_R = 4$, the NMSE performance difference is negligible even at the moderate B2B measurement SNR of 50 dB in the entire range of the field measurement SNR. It can be seen in Fig. 6-(b) that, with the large number of antennas $N_T = N_R = 64$, the moderate B2B measurement SNR of 50 dB may not be enough due to a large number of parameters to be estimated. However, the difference is negligible at high B2B measurement SNR of 70 dB in the entire range of the field measurement SNR. Such a high measurement SNR can be easily achieved by increasing the number L of observations in (6a). Note that the number of test channels is reduced from $N_T N_R = 4096$ to $N_T + N_R - 1 = 127$ by using the proposed method.

Fig. 7 compares the performance of the proposed system identification method and that of another conventional method in [19]. The proposed method is the same as Figs. 5 and 6. Now, the conventional method performs the B2B measurements with the same test channels as the proposed one. However, it ignores the crosstalk inside the Tx and Rx, i.e., it

in effect models the response matrices as diagonal matrices. Hence, in [19, Sec. 4], an N_R-by-N_T field measurement matrix is entry-by-entry divided by an estimated response matrix to compensate only for the linear distortion during the channel estimation. The conventional method suffers from detrimental NMSE degradation due to the ignored crosstalk, whereas our proposed method well estimates the channels over the entire range of the field measurement SNR.

VI. CONCLUSIONS AND FUTURE WORK

To efficiently calibrate the MIMO channel sounder with internal crosstalk, the LS system identification problem that utilizes only some B2B connections among all pairs of Tx and Rx ports is formulated. The notion of identifiability of the channel sounder is introduced and some optimal sets of B2B connections are found that minimize the number of B2B connections during the B2B measurements. The LS problem is converted to the weighted rank-one approximation problems in the frequency domain and solved by using the ACS algorithm. An initialization scheme is also proposed for the algorithm to converge within a couple of iterations. A propagation channel is then estimated from the field measurement data by using the estimated response matrices of Tx and Rx. The simulation results verify the effectiveness of the proposed calibration method.

In this paper, it is assumed that the internal crosstalk occurs only in the analog IF and RF sections, as it is the case with digital-IF or digital-RF channel sounders. However, for digital-baseband channel sounders, the crosstalk cannot be handled by two response matrices in complex baseband. The use of widely-linear system model [48] may be necessary to take into account the crosstalk among in-phase and quadrature paths in real baseband. A future work on such a sounder calibration problem is warranted.

Appendix

In this appendix, we derive the update functions in (22b) and (22c) of the proposed algorithm. Let $E[k]$ denote the objective function in (15) to be solved for k. Then, it can be rewritten as

$$E[k] = \sum_{(i,j)\in\mathbb{S}} \left\| \tilde{\boldsymbol{Z}}^{(i,j)}[k] - \tilde{\boldsymbol{U}}[k]\tilde{\boldsymbol{G}}^{(i,j)}[k]\tilde{\boldsymbol{V}}[k] \right\|_F^2 \quad (30\text{a})$$

$$= \sum_{(i,j)\in\mathbb{S}} \mathrm{tr}\Big\{ (\tilde{\boldsymbol{Z}}^{(i,j)}[k] - \tilde{\boldsymbol{U}}[k]\tilde{\boldsymbol{G}}^{(i,j)}[k]\tilde{\boldsymbol{V}}[k])^{\mathcal{H}}$$

$$(\tilde{\boldsymbol{Z}}^{(i,j)}[k] - \tilde{\boldsymbol{U}}[k]\tilde{\boldsymbol{G}}^{(i,j)}[k]\tilde{\boldsymbol{V}}[k]) \Big\}. \quad (30\text{b})$$

Since the derivative of (30b) with respect to $\tilde{\boldsymbol{V}}[k]$ is given by

$$\frac{\partial E[k]}{\partial \tilde{\boldsymbol{V}}[k]} = 2\left(\sum_{(i,j)\in\mathbb{S}} \tilde{\boldsymbol{G}}^{(i,j)}[k]^{\mathcal{H}} \tilde{\boldsymbol{U}}[k]^{\mathcal{H}} \tilde{\boldsymbol{U}}[k]\tilde{\boldsymbol{G}}^{(i,j)}[k] \right) \tilde{\boldsymbol{V}}[k]$$

$$-2\left(\sum_{(i,j)\in\mathbb{S}} \tilde{\boldsymbol{G}}^{(i,j)}[k]^{\mathcal{H}} \tilde{\boldsymbol{U}}[k]^{\mathcal{H}} \tilde{\boldsymbol{Z}}^{(i,j)}[k] \right), \quad (31)$$

we can find $\tilde{\boldsymbol{V}}[k] = \check{\boldsymbol{H}}_T(\tilde{\boldsymbol{U}[k]})$ as (22b) by solving $\partial E[k]/\partial \tilde{\boldsymbol{V}}[k] = 0$. The objective function $E[k]$ can be alternatively rewritten as

$$E[k] = \sum_{(i,j)\in\mathbb{S}} \mathrm{tr}\Big\{ (\tilde{\boldsymbol{Z}}^{(i,j)}[k] - \tilde{\boldsymbol{U}}[k]\tilde{\boldsymbol{G}}^{(i,j)}[k]\tilde{\boldsymbol{V}}[k])$$

$$(\tilde{\boldsymbol{Z}}^{(i,j)}[k] - \tilde{\boldsymbol{U}}[k]\tilde{\boldsymbol{G}}^{(i,j)}[k]\tilde{\boldsymbol{V}}[k])^{\mathcal{H}} \Big\}. \quad (32)$$

Since the derivative of (32) with respect to $\tilde{\boldsymbol{U}}[k]^{\mathcal{H}}$ is given by

$$\frac{\partial E[k]}{\partial \tilde{\boldsymbol{U}}[k]^{\mathcal{H}}} = 2\left(\sum_{(i,j)\in\mathbb{S}} \tilde{\boldsymbol{G}}^{(i,j)}[k]\tilde{\boldsymbol{V}}[k]\tilde{\boldsymbol{V}}[k]^{\mathcal{H}} \tilde{\boldsymbol{G}}^{(i,j)}[k]^{\mathcal{H}} \right) \tilde{\boldsymbol{U}}[k]^{\mathcal{H}}$$

$$-2\left(\sum_{(i,j)\in\mathbb{S}} \boldsymbol{G}^{(i,j)}[k]\tilde{\boldsymbol{V}}[k]\tilde{\boldsymbol{Z}}^{(i,j)}[k]^{\mathcal{H}} \right) \quad (33)$$

we can find $\tilde{\boldsymbol{U}}[k] = \check{\boldsymbol{H}}_R(\tilde{\boldsymbol{V}[k]})$ as (22c) by solving $\partial E[k]/\partial \tilde{\boldsymbol{U}}[k]^{\mathcal{H}} = 0$.

References

[1] 3rd Generation Partnership Project, 3GPP TS 36.211 v15.0.0, "Technical Specification Group Radio Access Network; Evolved Universal Terrestrial Radio Access (E-UTRA); Physical channels and modulation," release 15, Dec. 2017.

[2] 3rd Generation Partnership Project, 3GPP TS 38.211 v15.0.0, "Technical Specification Group Radio Access Network; NR; Physical channels and modulation," release 15, Dec. 2017.

[3] 3rd Generation Partnership Project, 3GPP TR 25.996 v9.0.0, "Spatial Channel Model for Multiple Input Multiple Output (MIMO) Simulations," release 9, Dec. 2009.

[4] 3rd Generation Partnership Project, 3GPP TR 36.873 V12.7.0, "Study on 3D channel model for LTE," release 12, Dec. 2017.

[5] N. Costa and S. Haykin, *Multiple-Input Multiple-Output Channel Models: Theory and Practice.* Hoboken, NJ, USA: Wiley, 2010.

[6] S. Salous, *Radio Propagation Measurements and Channel Modelling.* Hoboken, NJ, USA: Wiley, 2013.

[7] D. Chizhik, J. Ling, P. Wolniansky, R. Valenzuela, N. Costa, and K. Huber, "Multiple-input-multiple-output measurements and modeling in Manhattan," *IEEE J. Sel. Areas Commun.*, vol. 21, no. 3, pp. 321–331, Apr. 2003.

[8] Y. Yang, Y. Gui, H. Wang, W. Zhang, Y. Li, X. Yin, and C. X. Wang, "Parallel channel sounder for MIMO channel measurements," *IEEE Wireless Commun.*, vol. 25, no. 5, pp. 16–22, Oct. 2018.

[9] M. Kim, J. Takada, and Y. Konishi, "Novel scalable MIMO channel sounding technique and measurement accuracy evaluation with transceiver impairments," *IEEE Trans. Instrum. Meas.*, vol. 61, no. 12, pp. 3185–3197, Dec. 2012.

[10] Y. Chang, M. Ghoraishi, J. Takada, S. Suyama, and H. Suzuki, "Channel sounding technique using MIMO software radio architecture," in *Proc. 5th Eur. Conf. on Antennas and Propag. (EuCAP)*, Rome, Italy, Apr. 11–15, 2011, pp. 2546–2550.

[11] S. Salous, P. Filippidis, R. Lewenz, I. Hawkins, N. Razavi-Ghods, and M. Abdallah, "Parallel receiver channel sounder for spatial and MIMO characterisation of the mobile radio channel," *IEE Proc.-Commun.*, vol. 152, no. 6, pp. 912–918, Dec. 2005.

[12] S. Salous, S. M. Feeney, X. Raimundo, and A. A. Cheema, "Wideband MIMO channel sounder for radio measurements in the 60 GHz band," *IEEE Trans. Wireless Commun.*, vol. 15, no. 4, pp. 2825–2832, Apr. 2016.

[13] A. F. Molisch, F. Tufvesson, J. Karedal, and C. Mecklenbräuker, "A survey on vehicle-to-vehicle propagation channels," *IEEE Wireless Commun.*, vol. 16, no. 6, pp. 12–22, Dec. 2009.

[14] A. Paier, J. Karedal, N. Czink, H. Hofstetter, C. Dumard, T. Zemen, F. Tufvesson, A. F. Molisch, and C. F. Mecklenbräuker, "Car-to-car radio channel measurements at 5 GHz: Pathloss, power-delay profile and delay-Doppler spectrum," in *Proc. 7th IEEE Int. Symp. Wireless Commun. Syst. (ISWCS)*, Trondheim, Norway, Oct. 16–19, 2007, pp. 224–228.

[15] S. Sangodoyin, J. Salmi, S. Niranjayan, and A. Molisch, "Real-time ultrawideband MIMO channel sounding," in *Proc. 6th Eur. Conf. on Antennas and Propag. (EUCAP)*, Prague, Czech republic, Mar. 26–30, 2012, pp. 2303–2307.

[16] R. Wang, C. U. Bas, O. Renaudin, S. Sangodoyin, U. T. Virk, and A. F. Molisch, "A real-time MIMO channel sounder for vehicle-to-vehicle propagation channel at 5.9 GHz," in *Proc. IEEE Int. Conf. on Commun. (ICC)*, Paris, France, May 21–25, 2017, pp. 1–6.

[17] E. A. Lee, J. Kim, H.-J. Kim, Y.-J. Chong, and J. H. Cho, "Calibration of a fully-switched MIMO channel sounder with internal crosstalk," *Signal Process.*, vol. 156, pp. 21–30, Mar. 2019.

[18] V. Rabinovich and N. Alexandrov, *Antenna Arrays and Automotive Applications.* New York, NY, USA: Springer, 2012.

[19] Y. Chang, Y. Konishi, M. Kim, and J. Takada, "Calibration techniques for fully parallel 24×24 MIMO sounder," in *Proc. Int. Symp. on Antennas and Propag. (ISAP)*, Nagoya, Japan, Oct. 29–Nov. 2, 2012, pp. 331–334.

[20] J. Li, Y. Zhao, C. Tao, and B. Ai, "System design and calibration for wideband channel sounding with multiple frequency bands," *IEEE Access*, vol. 5, no. 1, pp. 781–793, Jan. 2017.

[21] G. R. MacCartney, Jr. and T. S. Rappaport, "A flexible millimeter-wave channel sounder with absolute timing," *IEEE J. Sel. Areas Commun.*, vol. 35, no. 6, pp. 1402–1418, June 2017.

[22] B. T. Maharaj, J. W. Wallace, M. A. Jensen, and L. P. Linde, "A low-cost open-hardware wideband multiple-input-multiple-output (MIMO) wireless channel sounder," *IEEE Trans. Instrum. Meas.*, vol. 57, no. 10, pp. 2283–2289, Oct. 2008.

[23] Y. Palaskas, A. Ravi, S. Pellerano, B. R. Carlton, M. A. Elmala, R. Bishop, G. Banerjee, R. B. Nicholls, S. K. Ling, N. Dinur, S. S. Taylor, and K. Soumyanath, "A 5-GHz 108-Mb/s 2×2 MIMO transceiver RFIC with fully integrated 20.5-dBm $P_{1\,\text{dB}}$ power amplifiers in 90-nm CMOS," *IEEE J. Solid-State Circuits*, vol. 41, no. 12, pp. 2746–2756, Dec. 2006.

[24] A. Abdelhafiz, L. Behjat, F. M. Ghannouchi, M. Helaoui, and O. Hammi, "A high-performance complexity reduced behavioral model and digital predistorter for MIMO systems with crosstalk," *IEEE Trans. Commun.*, vol. 64, no. 5, pp. 1996–2004, May 2016.

[25] C. Shan, L. Chen, X. Chen, and W. Wang, "A general matched filter design for reciprocity calibration in multiuser massive MIMO systems," *IEEE Trans. Veh. Technol.*, vol. 67, no. 9, pp. 8939–8943, Sep. 2018.

[26] R. Nie, L. Chen, C. Shan, and X. Chen, "A decentralized reciprocity calibration approach for cooperative MIMO," *IEEE Access*, vol. 7, pp. 1560–1569, Jan. 2019.

[27] K. Hausmair, U. Gustavsson, C. Fager, and T. Eriksson, "Modeling and linearization of multi-antenna transmitters using over-the-air measurements," in *Proc. IEEE Int. Symp. on Circuts Syst. (ISCAS)*, Florence, Italy, May 27–30, 2018, pp. 1–4.

[28] S. Hesami, S. R. Aghdam, C. Fager, T. Eriksson, R. Farrell, and J. Dooley, "Intra-Array coupling estimation for MIMO transceivers utilizing blind over-the-air measurements," in *Proc. IEEE MTT-S Int. Microw. Symp. (IMS)*, Boston, MA, USA, June 2–7, 2019, pp. 468–471.

[29] X. Wang, C. Yu, Y. Li, W. Hong, and A. Zhu, "Real-time single channel over-the-air data acquisition for digital predistortion of 5G massive

MIMO wireless transmitters," in *Proc. IEEE MTT-S Int. Wireless Symp. (IWS)*, Guangzhou, China, May 19–22, 2019, pp. 1–3.

[30] S. A. Bassam, M. Helaoui, and F. M. Ghannouchi, "Crossover digital predistorter for the compensation of crosstalk and nonlinearity in MIMO transmitters," *IEEE Trans. Microw. Theory Tech.*, vol. 57, no. 5, pp.1119–1128, May 2009.

[31] T. Sadeghpour, R. A. Alhameed, N. T. Ali, I. T. E. Elfergani, Y. Dama, and O. O. Anoh, "Linear and nonlinear crosstalk in MIMO OFDM transceivers," in *Proc. 18th IEEE Int. Conf. Electron., Circuits, Syst. (ICECS)*, Beirut, Lebanon, Dec. 11–14, 2011, pp. 504–507.

[32] S. Amin, P. N. Landin, P. Händel, and D. Rönnow, "Behavioral modeling and linearization of crosstalk and memory effects in RF MIMO transmitters," *IEEE Trans. Microw. Theory Techn.*, vol. 62, no. 4, pp. 810–823, Apr. 2014.

[33] A. Vaezi, A. Abdipour, A. Mohammadi, and F. M. Ghannouchi, "On the modeling and compensation of backward crosstalk in MIMO transmitters," *IEEE Trans. Microw. Wireless Compon. Lett.*, vol. 27, no. 9, pp. 842–844, Sep. 2017.

[34] H. Qian, X. Cheng, X. Luo and W. Feng, "Calibration of nonlinear crosstalk in MIMO transmitter," *IEEE Trans. Veh. Technol.*, vol. 66, no.5, pp. 3739–3748, May 2017.

[35] K. Hausmair, P. N. Landin, U. Gustavsson, C. Fager, and T. Eriksson, "Digital predistortion for multi-antenna transmitters affected by antenna crosstalk," *IEEE Trans. Microw. Theory Techn.*, vol. 66, no. 3, pp. 1524–1535, Mar. 2018.

[36] Z. A. Khan, E. Zenteno, P. Händel, and M. Isaksson, "Extraction of the third-order 3x3 MIMO Volterra kernel outputs using multitone signals," *IEEE Trans. Microw. Theory Techn.*, vol. 66, no. 11, pp. 4985–4999, Nov. 2018.

[37] P. Händel and Rönnow, "MIMO and massive MIMO transmitter crosstalk," *IEEE Trans. Wireless Commun.*, vol. 19, no. 3, pp. 1882–1893, Mar. 2020.

[38] Arun K. Tangirala, *Principles of System Identification: Theory and Practice.* Boca Raton, FL, USA: CRC Press, 2014.

[39] N. Srebro and T. Jaakkola, "Weighted low-rank approximations," in *Proc. 20th Int. Conf. Mach. Learn. (ICML)*, Washington, DC, USA, Aug. 21–24, 2003, pp. 720–727.

[40] E. Lehmann and G. Casella, *Theory of Point Estimation.* New York: Springer Verlag, 1998.

[41] R. J. Gould, "Advances on the Hamiltonian Problem," *Graphs and Combinatorics*, vol. 19, no. 1, pp. 7–52, Mar. 2003.

[42] I. Markovsky, *Low Rank Approximation: Algorithms, Implementation, Applications.* London, U.K.: Springer, 2011.

[43] J. Gorski, F. Pfeuffer, and K. Klamroth, "Biconvex sets and optimization with biconvex functions: A survey and extensions," *Math. Meth. Oper. Res.*, vol. 66, no. 6, pp. 373–407, Dec. 2007.

[44] Mini-circuits, "SP6T RF switch," JSW6-33DR+ datasheet.

[45] M. Taranetz, T. Blazek, T. Kropfreiter, M. K. Muller, S. Schwarz, and M.Rupp, "Runtime precoding: Enabling multipoint transmission in LTE-advanced system-level simulations," *IEEE Access*, vol. 3, pp. 725–736, June 2015.

[46] N. K. Kumar and J. Schneider, "Literature survey on low rank approximation of matrices," *Linear Multilinear Algebra*, vol. 65, no. 11, pp. 2212–2244, Dec. 2016.

[47] G. H. Golub and C. F. Van Loan, *Matrix Computations.* Baltimore, MD, USA: Johns Hopkins Univ. Press, 1996.

[48] P. J. Schreier and L. L. Scharf, *Statistical Signal Processing of Complex-Valued Data: The Theory of Improper and Noncircular Signals.* Cambridge, U.K.: Cambridge Univ. Press, 2010.

Junseonk Kim (M'20) received the B.S. and M.S. degrees in Electrical Engineering from Pohang University of Science and Technology (POSTECH), Pohang, Korea, in 2017 and 2019, respectively. Since 2019, he has been with the Electronics and Telecommunications Research Institute (ETRI), Daejeon, Korea. His research interests include radio propagation, wireless channel measurement and modeling, and 5G physical layer specifications.

Eun Ae Lee received B.S. and M.S./Ph.D. degrees in Electrical Engineering from POSTECH in 2010 and 2019, respectively. Since 2019, she has been with Samsung Electronics Co., Ltd., Hwaseong, Korea. Her research interests include adaptive signal processing, circuit measurement and modeling, and DRAM circuit design.

Chung-Sup Kim received the B.S. and M.S. degrees in Electrical Engineering from Kyungpook National University, Daegu, Korea, in 1997 and 1999, respectively. Since 1999, he has been with ETRI and currently working as the principal researcher. His research interests include direction finding, beamforming, RADAR, radio propagation, and 5G communication.

Young-Jun Chong received the B.S. degree from the Jeju University, Jeju, Korea, in 1992, the M.S. degree in electronics engineering from the Sogang University, Seoul, Korea, in 1994, and the Ph.D. degree in electronic engineering from the Chungnam National University, Daejeon, Korea, in 2005, respectively. Since 1994, he has been with ETRI, where he is a principle member of the research staff of the Radio Resource Research Section. He served as a project leader involved in the research of spectrum engineering. His research interests include RF circuit and systems, radio interference, mobile communications, and interference modeling. He is a member of KIEES.

Joon Ho Cho (S'99–M'01) received the B.S. degree (summa cum laude) in Electrical Engineering from Seoul National University, Seoul, Korea, in 1995 and the M.S.E.E. and Ph.D. degrees in Electrical and Computer Engineering from Purdue University, West Lafayette, IN, in 1997 and 2001, respectively.

From 2001 to 2004, he was with the University of Massachusetts at Amherst as an Assistant Professor. Since 2004, he has been with POSTECH, where he is presently an Associate Professor in the Department of Electrical Engineering. His research interests include waveform design, multiuser communications, MIMO signal processing, channel measurement and modeling, and information theory.

Dr. Cho served as an Associate Editor for the IEEE TRANSACTIONS ON VEHICULAR TECHNOLOGY and served as the Vice President for Admissions and Student Affairs of POSTECH.